TRG Report 1213 (S)

United Kingdom Atomic Energy Authority

THE IRRADIATION BEHAVIOUR OF URANIUM CARBIDE/SILICON CARBIDE DISPERSED FUELS

J. V. SHENNAN
Reactor Fuel Element Laboratory
Springfields

F. STERRY and H. J. DeNORDWALL
Atomic Energy Research Establishment
Harwell

1966

THE REACTOR GROUP
HQ, Risley, Warrington, Lancs

Obtainable from H.M. Stationery Office
Seven Shillings Net

R2193

TRG Report 1213(S)

THE IRRADIATION BEHAVIOUR OF URANIUM CARBIDE/SILICON CARBIDE DISPERSED FUELS

by

J.V. Shennan, F. Sterry and H.J. DeNordwall

SUMMARY

The irradiation behaviour of UC/SiC dispersed fuel rods incorporating silicon carbide and pyrocarbon coated uranium carbide spheres has been investigated in low- and high-temperature capsules in the Dounreay Materials Testing Reactor and also in the HTGC loop in the PLUTO reactor at Harwell.

Excellent results have been obtained for fuel rods containing pyrocarbon coated particles in all three types of experiment. For example, the capsule irradiation in an HPD rig at 1200°C was taken to a burn-up of 44,000 MWd/te at a rating of 1 kW/in without any microscopic damage to the specimens, and microstructural examination revealed no irradiation damage other than the classical 'spearhead' attack in the inner layers of the pyrocarbon coatings. Similar fuel irradiated in the PLUTO loop at a maximum rating of 1 kW/in at 1250°C gave R/B for Xe133 of $\sim 4 \times 10^{-6}$, and post-irradiation examination again revealed no significant change in the external appearance of the six specimens. Radiochemical examination of the loop components has been made, but the surface concentrations of all fission products were often too low to measure and much longer experiments would be necessary to assess any time dependence of fission-product release and to obtain more complete distribution information.

Irradiations of fuel containing silicon carbide coated particles have generally suffered from overheating effects in both HPD and PLUTO loop experiments, when cracking of the silicon carbide matrix occurs under the stresses produced by cycling the rods through the melting point of silicon (1410°C). However, irradiation results at low temperatures (700-800°C) suggest that silicon carbide coated fuel is inferior to pyrocarbon coated fuel. Metallographic examination reveals a much greater extent of matrix cracking, the cracks apparently being initiated at the coat-kernel interface, and there was an associated increase in the release of fission products. It is thought that cracking results from stresses set up in the inner layers of the coat by fission-fragment damage, which in the case of pyrocarbon are relieved by densification processes resulting in the phenomenon of 'spearhead' attack.

The text of this Report was presented as a paper to the DRAGON Contractors' Research and Development Symposium, AERE, Harwell, March, 1966.

Draft submitted by authors: 28 June 1966

Draft received at Risley for issue: 12 July 1966

C.15

U.D.C. Nos.
621.039.542.344

CONTENTS

INTRODUCTION

1. The development of a coated-particle dispersed fuel for use in an AGR system has been discussed recently by D'Eye,[1] who also reviews the results of an economic assessment of such a fuel and outlines the main stages of the fabrication processes. Two dispersed-fuel concepts based on a dense, self-bonded silicon carbide matrix emerged from the early fabrication studies. The first concept comprised a dispersion of silicon carbide coated, uranium monocarbide spheres in a silicon carbide matrix. In the second, the matrix incorporated pyrolytic carbon coated, uranium dicarbide spheres. In terms of fabrication there are advantages and disadvantages in both systems, but the choice of fuel concepts for further development obviously rests on the comparative irradiation performance of the two fuels. Thus, an irradiation programme was devised to test the two fuels.

2. The irradiation experiments fall into three categories:

(a) Capsule irradiations of fuel pins at low temperatures, 700-800°C (IE 269).
(b) Capsule irradiations of fuel pins at high temperatures, 1000-1200°C (IE 309).
(c) Irradiation of fuel pins in the PLUTO High-temperature Gas-cooled Loop.

Capsule tests give information on the mechanical stability of the fuel and on the incidence of irradiation damage. The irradiations were performed in the Materials Testing Reactor at Dounreay (DMTR) and post-irradiation examinations were made by the Ceramic Fuel Group at Windscale. Irradiation experiments in the PLUTO loop give similar post-irradiation information but, more important, provide a measure of the retentivity of the fuel by means of R/B values* obtained by continual sampling of the coolant gas for short-lived isotopes of xenon and krypton. In addition, information as to the fractional release of iodine and metallic fission products is provided by a post-irradiation radiochemical analysis of the loop components. All operations connected with the PLUTO loop experiments, including post-irradiation examination, were performed at AERE, Harwell.

3. Because a PLUTO loop experiment presents such a complete picture of the irradiation performance of the test fuel, the results of the irradiation programme have been presented in this Report chiefly in terms of the three PLUTO charges examined. The results from the capsule tests have been incorporated at suitable points to provide additional or confirmatory information.

DETAILS OF SPECIMENS

4. The preparation of UC/SiC fuel rods has already been described,[2] and specimens for most irradiation experiments have been made from 0·5 in. dia. extrusions having a nominal fuel core diameter of 0·39 in. Specimens for the PLUTO loop had an overall length of 6 in., including 0·05 in. unfuelled end-caps at each end which were grooved to fit thermocouples. Three specimens in the loop charge of six were grooved circumferentially at the centre to allow surface temperatures to be measured directly (Fig. 1). Specimens irradiated in the low- and high-temperature capsules were generally 3 in. long with a fuel-core length of 2·75 in. Details of the coated particles and fuel loading for the experiments are given in Table I.

PLUTO CHARGE 9

5. The specimens for this experiment were made in September 1964, when many fabrication problems remained to be solved. In particular, the need to control the siliconising temperature

*The R/B value is the ratio of release rate to birth rate for a particular fission product.

TABLE I

Details of fuel in irradiation specimens

IE No.	Irradiation rig	Specimen		
		Type	Fuel concentration, g/cm^3	Enrichment, %
309/3	HPD rig*	60 μ pyrolytic graphite on 490 μ UC_2 kernel. 40 vol.% dispersion in SiC matrix	1·72	22
309/4	HPD rig*	180 μ SiC coat on 480-500 μ UC kernel. 40 vol.% dispersion in SiC matrix	0·82	24·5
269/3	Type 101	As for IE 309/3	1·72	22
269/4	Type 101	As for IE 309/3	1·72	22
269/5	Type 103	As for IE 309/4	0·82	24·5
269/6	Type 103	As for IE 309/4	0·81	24·5
Pluto 9	PLUTO loop	180 μ SiC coat on 480-500 μ UC kernel. 40 vol.% dispersion in SiC matrix	0·81	24·5
Pluto 10	PLUTO loop	180 μ SiC coat on 480-500 μ UC kernel. 40 vol.% dispersion in SiC matrix	0·81	24·5
Pluto 13	PLUTO loop	65 μ pyrolytic graphite coat on 440 μ UC_2 kernel. 40 vol.% dispersion in SiC matrix.	1·62	19·95

*High power density rig

was not recognised, and temperatures were allowed to reach the level where considerable reaction occurred between the UC kernel and the silicon carbide coating. This reaction, which affected all particles to some degree, leads to penetration of the coating by uranium silicides and the formation of UC_2 and SiC in the kernel. In the worst cases the reaction front extended half-way through the coating (Fig. 2). In addition, the level of uranium contamination of the matrix, probably concentrated in the free silicon, was high, as indicated by the amounts of uranium leached from the rods and the final α-assay (Table II).

PLUTO CHARGE 10

6. The specification for this charge was the same as for Charge 9, but the fabrication of the specimens was carefully controlled to reduce the levels of contamination and the UC-SiC reaction. The nitric acid leach results (Table III) and the microstructure of Fig. 3 show the extent of the improvement achieved.

TABLE II

Uranium contamination in PLUTO Charge 9 specimens

Position	Rod no.	Wt. of U leached from rod in 3-h period, μg			α count, dpm
		1st	2nd	3rd	
Inlet	13	42	54	53	865
↓	22	2000	79	112	990
	9	37	<25	55	488
	15	2100	134	63	1180
	8	<25	78	1200	575
Outlet	11	2500	103	77	1290

TABLE III

Uranium contamination in PLUTO Charge 10 specimens

Position	Rod no.	Wt. of U leached from rod in 3-h period, μg			α count, dpm
		1st	2nd	3rd	
Inlet	6	720	<25	<25	Average count on spares 65 dpm
↓	5	1580	<25	<25	
	4	<25	<25	<25	
	3	<25	<25	<25	
	2	46	<25	<25	
Outlet	1	760	<25	<25	

PLUTO CHARGE 13

7. The specimens in this charge contain pyrocarbon coated UC_2 spheres in which there is no bonding of the kernel to the coating. However, some reaction between silicon and the outer layers of the coating occurs in the siliconising process, giving a dense β-SiC zone around the coating which serves to bond the particle to the matrix. The microstructure of Fig. 4 shows the typical features of this fuel, namely the duplex coating, the gap between coating and dense UC_2 kernel and the reaction zone around the particle. The contamination levels in the specimens (Table IV) are similar to those for Charge 10, but examination of the α-counts indicates there is still room for improvement in matrix contamination.

DETAILS OF IRRADIATION RIGS AND OPERATION

LOW-TEMPERATURE CAPSULES

8. The specimens are contained in an inner stainless-steel container which is surrounded by a copper sleeve. A predetermined helium-filled gas gap between the copper sleeve and the outer stainless-steel capsule is the main control of heat transfer to the reactor coolant.

TABLE IV

Uranium contamination in PLUTO Charge 13 specimens

Position	Rod no.	Wt. of U leached from rod in 3-h period, μg			α count, dpm
		1st	2nd	3rd	
Inlet	2	<25	<25	40	150
↓	3	<25	<25	<25	550
	4	348	<25	<25	250
	6	<25	<25	<25	400
	7	510	<25	<25	350
Outlet	8	<25	<25	<25	250

Thermocouples are located in the copper sleeve, and specimen temperatures estimated from the heat-transfer data. The capsules (Dounreay design, types 101 and 103) were designed to give surface temperatures of 800°C and linear ratings of 700-750 W/in. These conditions have been achieved for both fuel concepts and mean burn-ups of 4% and 5% FIMA* have been obtained with pyrocarbon and silicon carbide fuel respectively (IE 269/4, 269/6).

HIGH-TEMPERATURE CAPSULES

9. The high-temperature capsule was, in fact, a modified form of the Dragon Project HPD rig, in which the specimens (generally three) were located in cylindrical graphite boxes. Again, no direct measurement of temperatures was made, but these were estimated from heat-transfer measurements. The details of the rig were designed to allow high fuel ratings, up to 1300 W/in, and surface temperatures up to 1150°C. The high ratings were achieved but the associated high temperature gradients and the uncertainties of the gas gap between specimen and fuel box led to inaccurate estimates of fuel temperature, and in several experiments, unfortunately involving SiC-coated particle fuel in every case, serious overheating occurred.

PLUTO LOOP

10. The test section for UC/SiC irradiations is shown diagrammatically in Fig. 5. The six rods were placed end-to-end in a stainless-steel tube and supported along the axis by wire triangles of stainless steel in Charges 9 and 10, and Chromel in Charge 13. The change in the material for the support wires was occasioned by post-irradiation evidence of reaction between stainless steel and silicon carbide at the higher temperatures, while the Chromel thermocouples were unaffected. The rods were cooled directly by helium at 10 atm pressure. A fraction of the main coolant was passed through a clean-up section to remove impurities, such that the total circuit volume passed through the clean-up section in half an hour.

11. The loop irradiations were designed to give maximum linear ratings of 750-1000 W/in and a maximum surface temperature of 1150°C. It was intended to measure surface and fuel temperatures by thermocouples fitted into the grooves in the rods. In practice thermocouple readings were closer to gas temperatures than rod temperatures, and surface temperatures were therefore estimated from measurements of gas flow and gas temperatures using a heat-transfer correlation which has been verified as applicable to similar loop test assemblies, namely:

$$\text{Stanton no.} \times (\text{Reynolds no.})^{0\cdot2} \times (\text{Prandtl no.})^{0\cdot6} = 0\cdot035$$

A typical temperature distribution is shown in Fig. 5.

*FIMA = fissions per initial metal atoms.

PLUTO CHARGE 9

12. The specimens in this first charge received three irradiation cycles, 80 days, at a mean loop power of 16 MW which corresponded with a maximum rating of 600 W/in. Difficulties with the secondary coolant kept the temperature below 1000°C for the first cycle, but the maximum temperature reached 1500°C at the start of the second cycle, falling rapidly to an average value of 1300°C. The average temperature for the third cycle was 1250°C. The calculated mean burn-up was 2·3% F I M A.

PLUTO CHARGE 10

13. This experiment ran for four reactor cycles, 93 days, at an increased power of 20 MW. Surface temperatures were again estimated and, initially at least, were well above the design values. The mean values for the maximum fuel surface temperatures were:

first cycle	1362°C	second cycle	1252°C
third cycle	1246°C	fourth cycle	1222°C

The calculated mean burn-up was 3·2% F I M A.

PLUTO CHARGE 13

14. The fuel loading was almost doubled in this experiment so that the loop power was about 30 MW, giving a maximum rating of 1 kW/in. Temperatures were fairly steady throughout the three cycles of irradiation, 62 days, and the average maximum surface temperatures were respectively 1290°, 1270° and 1217°C. Unlike the two previous experiments where the helium coolant purity was very high and constant throughout, the first irradiation in Charge 13 was made with a coolant composition of 1 part air, 9-10 parts helium. The presence of air was due to a malfunctioning of valves during the preliminary loop evacuation; it was removed by re-evacuation of the loop before the second irradiation period. The calculated mean burn-up was 1·6% F I M A.

IRRADIATION PERFORMANCE OF UC/SiC FUEL RODS CONTAINING SiC COATED PARTICLES

15. As already mentioned, all the high-temperature capsule irradiations involving this fuel concept overheated, and estimated fuel centre temperatures exceeded 1500°C. All specimens failed badly because of a phenomenon unrelated to irradiation damage and referred to as the 'silicon melting effect'. Because this phenomenon probably affected the PLUTO loop irradiations to some extent, it is useful to describe it briefly here.

FAILURE DUE TO CENTRE MELTING OF SILICON

16. The self-bonded silicon carbide matrix contains up to 10 vol.% free silicon, and silicon undergoes a volume change on melting (m.p. 1410°C), the density of molten silicon being greater than that of crystalline silicon by about 10%. When a silicon carbide rod is heated directly, either by fission or by electric current, a temperature gradient is established and, when temperatures in the central regions of the rod exceed the silicon melting point, silicon will be drawn up the temperature gradient towards the centre to fill the newly-created porosity. When the power is cut off, the outer regions of the rod cool more quickly, and solidification of the silicon in these regions restricts the expansion of the silicon in the central regions during further cooling. Thus a large strain is created which causes the rod to crack and the excess silicon to be ejected with some force from the central regions. These features have been well demonstrated in out-of-pile electrical heating experiments, and

ceramographic evidence (Fig. 6) confirms the above mechanism. Further temperature cycling, e.g. due to reactor trips and shut-downs, leads to extensive cracking, penetration of the kernels by liquid silicon with the formation of uranium silicides, and the dispersion of uranium probably as a silicon-silicide eutectic throughout the matrix. All these effects were observed by Livesey's post-irradiation examination team at Windscale on HPD irradiations of fuel containing SiC-coated particles (e.g. IE 309/4). Figure 7 shows a typical specimen from IE 309/4, having a major crack and silicon concentration.

17. Useful irradiation data have been obtained from low-temperature capsule experiments, but these results will be discussed together with those from the two PLUTO experiments.

PLUTO CHARGE 9

18. During irradiation, samples of loop gas were taken regularly and analysed by gamma-ray spectrometry to determine the concentrations of the shorter-lived isotopes of xenon and krypton. These results were converted to R/B values and the mean for each cycle, corrected for variations in the average loop power from cycle to cycle, is shown in Table V.

TABLE V

Average fission-gas release from PLUTO Charge 9

Cycle	Xe133	Xe135	Kr85m	Kr88	Kr87
1	$8{\cdot}75 \times 10^{-4}$	$2{\cdot}12 \times 10^{-4}$	$2{\cdot}15 \times 10^{-4}$	$2{\cdot}14 \times 10^{-4}$	$8{\cdot}54 \times 10^{-5}$
2	$1{\cdot}29 \times 10^{-3}$	$4{\cdot}92 \times 10^{-4}$	$3{\cdot}06 \times 10^{-4}$	$2{\cdot}64 \times 10^{-4}$	$1{\cdot}94 \times 10^{-4}$
3	$1{\cdot}81 \times 10^{-3}$	$6{\cdot}17 \times 10^{-4}$	$7{\cdot}20 \times 10^{-4}$	$5{\cdot}65 \times 10^{-4}$	$2{\cdot}94 \times 10^{-4}$

19. The initial gas release is high and there is a gradual increase in the release rate, which is further illustrated in the plot of R/B for Xe133 against time shown in Fig. 8. It is believed that the high initial release is associated with the high level of uranium contamination of these specimens, but the steady increase must be due to continuous cracking of the coatings and the matrix. In fact, post-irradiation examination revealed that most of the rods were cracked in axial and circumferential directions, this crazing being most marked for specimen 11 located adjacent to the helium outlet tube (Fig. 9). Ceramographic examination of sections of the coldest rod (no. 6) at the helium inlet end, revealed extensive radial cracking in the silicon carbide coats, appearing to be initiated in the UC-SiC reaction zone but penetrating into the matrix (Fig. 10). Similar results have been obtained from the capsule irradiations (e.g. IE 269/6), where specimens taken to 5% burn-up were so brittle that sectioning tended to cause break-up of the rods. The general crazing of the fuel is shown in Fig. 11.

PLUTO CHARGE 10

20. The average releases of xenon and krypton isotopes are shown in Table VI, and while they show some improvement over Charge 9 results, the average values tend to obscure the nature of the change of R/B with time. Again, a plot of R/B for Xe133 against time has been made (Fig. 8). The large reduction in contamination achieved in these specimens is manifested in the low release, 6×10^{-6}, of the first seven days of irradiation. The improvement was short-lived, however, for after a week there was a sudden increase, by an order of magnitude, in the release. The release rate remained fairly steady in the second cycle, although the level was somewhat lower at $1\text{-}2 \times 10^{-5}$, presumably associated with the fall in temperature of 100 degC. The beginning of the third cycle marked a second sharp increase in R/B to 10^{-4}, which was followed by a steady rise during the remaining 30 days' irradiation to a final value of $1\text{-}2 \times 10^{-3}$.

TABLE VI

Average fission-gas release from PLUTO Charge 10

Cycle	Xe133	Xe135	Kr85m	Kr88
1	$4{\cdot}30 \times 10^{-5}$	$8{\cdot}10 \times 10^{-6}$	$1{\cdot}77 \times 10^{-5}$	$6{\cdot}50 \times 10^{-6}$
2	$1{\cdot}60 \times 10^{-5}$	$1{\cdot}11 \times 10^{-5}$	$1{\cdot}30 \times 10^{-5}$	$4{\cdot}74 \times 10^{-6}$
3	$1{\cdot}04 \times 10^{-4}$	$1{\cdot}85 \times 10^{-5}$	$9{\cdot}00 \times 10^{-5}$	$4{\cdot}52 \times 10^{-5}$
4	$3{\cdot}22 \times 10^{-4}$	$6{\cdot}24 \times 10^{-5}$	$1{\cdot}89 \times 10^{-4}$	$8{\cdot}84 \times 10^{-5}$

21. Post-irradiation examination revealed none of the surface crazing of Charge 9, but one of the hotter rods, no. 4, had broken in two at the central groove and there was a major radial crack extending end to end in one of the broken halves. Ceramographic examination revealed that there was a smaller incidence of matrix cracking in the surface of this radial crack (Fig. 12) than below it, where cracking of coatings and matrix was similar to those observed in Charge 9 specimens.

DISCUSSION OF RESULTS ON SiC-COATED PARTICLE FUEL

22. The first important result obtained from this irradiation programme and subsequently confirmed in out-of-pile evaluation is that a centre temperature limitation of this fuel is set by the 'silicon melting effect'. This limit is probably about 1500°C to allow for a sufficiently wide central melting zone.

23. The large gas release and associated cracking in the Charge 9 specimens, however, cannot be attributed to silicon melting, for the high release was obtained at the beginning of irradiation, when the maximum temperature was less than 1000°C. Furthermore, although the temperature of the more highly rated specimens reached 1500°C in the second cycle, cracking extended to the colder rods whose temperature probably never exceeded 1000°C for the whole of the irradiation period. In Charge 10 the initial temperature conditions would have caused centre melting of silicon in the hottest specimen, and the reactor trip which occurred on the 5th day could have initiated the crack in rod 4, which would explain the first sharp increase in R/B. The second increase in release could then be caused by an extension of the crack after the repeated temperature cycling due to trips and shutdowns but, again, the final steady increase in R/B with time could only be caused by continual cracking of the coatings and matrix.

24. Thus, perhaps the most important result of these experiments was the ceramographic evidence of a high proportion of cracked coats whose cracks penetrated the matrix to such an extent that many particles were linked together by cracks. Because of this concentrated network of cracks in the fuel core, only a small number of paths through the fuel-free layer would be required to produce a large fractional release of fission gases. Further, if a major radial crack occurs in the fuel core, as in Charge 10, a free surface is immediately available within the cracked particle network and release is unimpeded.

25. The source of the cracks is probably in the inner layers of the SiC coating adjacent to the kernel, heavily damaged by fission fragments (Fig. 13). The required growth of the silicon carbide inner layers which cannot be accommodated in the fully dense coating, combined with the large restraint applied by the strong silicon carbide matrix, would lead to high stresses and eventually to rupture. It is noteworthy that the matrix in the surface of the crack, in the broken specimen from Charge 10, showed a smaller incidence of cracking, presumably because expansion of the coatings in the crack surface could more easily occur once the matrix restraint had been removed.

IRRADIATION PERFORMANCE OF UC/SiC FUEL RODS CONTAINING PYROCARBON COATED PARTICLES

26. In marked contrast to the first concept fuel, excellent irradiation results have been obtained with silicon carbide rods containing pyrocarbon coated particles. In the HPD rig, IE 309/3, specimens were taken to a burn-up of ~ 4% at a linear rating of 1 kW/in and a surface temperature of 1200°C. The matrix was unaffected and damage was confined to the low-temperature inner pyrocarbon coating producing the classical 'spearhead' attack (Fig. 14). Equally successful irradiations were performed in the low-temperature capsules (i.e. IE 269/3, 4) at 800°C, burn-ups being taken to 5%, which would be the design value for this fuel concept in an AGR . The superiority of this fuel is, however, best demonstrated by its performance in the PLUTO loop experiment, Charge 13.

PLUTO CHARGE 13

27. As in the previous charges, samples of the gas in the main circuit were analysed for fission-product release. In the first irradiation period no gamma spectrum of Xe and Kr was obtained on the day of sampling, the spectra being masked by a large Ar41 peak arising from the presence of air in the coolant. After the sample had cooled for 24 h, a small Xe133 peak still remaining gave a fractional release of 2×10^{-6} and it may have been less. When the air was removed from the loop in the second and third cycles, it was possible to obtain R/B values for the Xe and Kr isotopes as before; the mean values are given in Table VII. The plot of R/B for Xe133 against time (Fig. 8), in contrast to the two upper curves for Charges 9 and 10, shows that the release rate is fairly constant at the low level of $\sim 4 \times 10^{-6}$.

TABLE VII

Average fission gas release from PLUTO Charge 13

Cycle	Xe133	Xe135	Kr85m	Kr88
1	$2{\cdot}00 \times 10^{-6}$	-	-	-
2	$4{\cdot}16 \times 10^{-6}$	$8{\cdot}25 \times 10^{-7}$	$3{\cdot}46 \times 10^{-6}$	$1{\cdot}55 \times 10^{-6}$
3	$4{\cdot}64 \times 10^{-6}$	$9{\cdot}68 \times 10^{-7}$	$5{\cdot}10 \times 10^{-6}$	$2{\cdot}32 \times 10^{-6}$

28. Post-irradiation examination showed little visible deterioration (Fig. 15), apart from chips in the end caps of some of the rods and a small fine crack running in about ½ in. from such a chip in the coldest rod. Ceramographic examination in general confirmed the results from the capsule experiments, although one section revealed a small crack. The latter, however, tended to run round the coated particles rather than through them and, in fact, only one particle was breached by the crack.

DISCUSSION OF RESULTS ON PYROCARBON COATED FUEL

29. It has been concluded that the poorer irradiation results of the first concept fuel arise from the inability of the silicon carbide coating to accommodate the displacements caused by fission fragments. Conversely, the superior nature of the pyrocarbon coated fuel, well demonstrated in this irradiation programme, is due to the ability of the low-density pyrocarbon to absorb the fission-fragment damage by the process of densification producing the 'spearhead attack'. The matrix is then subjected only to the pure thermal stresses arising from the temperature gradient.

30. It may be possible to prepare a duplex silicon carbide coated particle with a sufficiently low-density inner SiC layer to accommodate the fission-fragment damage. It is certainly possible to prepare a duplex carbon-silicon carbide coated particle as in the DRAGON fuel, but it is difficult to see the advantages of this particle over the pyrcarbon system when incorporated in a dense self-bonded silicon carbide matrix.

RELEASE OF IODINE AND METALLIC FISSION PRODUCTS FROM UC/SiC FUEL RODS

31. The fractional release of metallic fission products from UC/SiC fuel has been determined for the three loop experiments by post-irradiation radiochemical analysis of the loop components swept by the coolant gas. On entering the fuel element section the coolant passes between the cylindrical fuel element and a stainless wall which would represent the fuel element channel wall in the reactor. After the fuel, the gas passes through a short graphite tube into the shield plug section, in which there is some cooling, and finally into a water-cooled heat exchanger. Pieces of this circuit from all parts, except the heat exchanger, were analysed at Harwell and Woolwich for deposited fission-product activity.

CONTAMINATION

32. Contamination by U235 before or during irradiation or by irradiated fuel during dismantling is monitored by Zr95 analyses. Equivalent activities of other fission products are assumed to accompany the Zr95, and these are subtracted from the observed fission-product activities to give 'corrected' values.

TOTAL FISSION-PRODUCT ACTIVITIES FOUND

33. The fractions of the activities present at shut-down are listed in Tables IX-XX (at the end of the Report), and the calculated fractional releases for the various nuclides are shown in the histogram, Fig. 16. In the last experiment, Charge 13, the fission-product activity was substantially lower than that arising from the activation of stainless-steel constituents.

DISTRIBUTION OF METALLIC FISSION PRODUCTS

34. Caesium behaved differently from the other metallic fission products. Its release was ~100 times higher than that of any other fission product, and its distribution was far less uniform in the stainless-steel part of the primary circuit, the majority having deposited in the shield plug section, and presumably in the heat exchanger which could not be sampled.

35. Strontium, barium, yttrium and cerium, where they could not be ascribed to contamination, were approximately uniformly distributed. Such uniform distributions have been taken to indicate release from the fuel as gaseous precursors rather than metals, since the coolant circulates in a time which is short compared with the half-lives of these nuclides' precursors. Comparisons of the releases of caesium, strontium and barium with the releases of their precursors tend to confirm this view. It was not possible to measure R/B for the short-lived precursors during the loop operation, and these values have therefore been estimated on the assumption that R/B varied with $\lambda^{-\frac{1}{2}}$. The release of caesium is > 1000 times that of Xe137, whereas others are much closer, particularly in Charge 9 (Table VIII). The fraction of activity released as metal increased as the release itself fell. This seems consistent with smaller discontinuities in the matrix creating larger delays, and the known behaviour of pyrocarbon which transmits Group II metals but retains the noble gases.

TABLE VIII

Comparison of precursor and daughter activities

Daughter nuclide	Fractional release					
	Charge 9		Charge 10		Charge 13	
	Gas	Metal	Gas	Metal	Gas	Metal
Cs137	$3{\cdot}6 \times 10^{-5}$	$2{\cdot}0 \times 10^{-3}$	$4{\cdot}0 \times 10^{-6}$	$1{\cdot}0 \times 10^{-3}$	$9{\cdot}0 \times 10^{-8}$	$9{\cdot}0 \times 10^{-5}$
Sr89	$4{\cdot}5 \times 10^{-5}$	$2{\cdot}1 \times 10^{-5}$	$1{\cdot}3 \times 10^{-5}$	$3{\cdot}2 \times 10^{-6}$	$3{\cdot}8 \times 10^{-7}$	$2{\cdot}8 \times 10^{-8}$
Sr90	$1{\cdot}5 \times 10^{-5}$	$3{\cdot}2 \times 10^{-5}$	$5{\cdot}4 \times 10^{-6}$	$3{\cdot}6 \times 10^{-5}$	$1{\cdot}6 \times 10^{-7}$	$1{\cdot}5 \times 10^{-6}$
Ba140	$1{\cdot}0 \times 10^{-5}$	$9{\cdot}0 \times 10^{-6}$	$1{\cdot}0 \times 10^{-6}$	$2{\cdot}0 \times 10^{-6}$	$2{\cdot}0 \times 10^{-8}$	$1{\cdot}0 \times 10^{-6}$

RELEASE AND DISTRIBUTION OF IODINE AND TELLURIUM

36. Release of iodine was less than that of Xe133 at the end of the experiments. The difference between the I131 and Xe133 releases was accentuated when the Xe133 release was increasing rapidly, as in Charge 9.

37. When the iodine concentration was high, a remarkably large fraction of the iodine plated-out on the fuel channel sleeve within a few centimetres of its probable point of origin, as shown by the small "lag" of the iodine distribution behind the fuel temperature distribution. In Charge 13 no iodine could be detected on the fuel channel wall, and so little was found in the external circuit that it would be invidious to make any comment as to whether this useful decontamination was still applicable.

38. The fractional release of tellurium (Te129m) was less than that of I131 where both were measurable.

CONCLUSIONS

39. The measurements of fission-gas release and the results of the visual and ceramographic post-irradiation examinations obtained in the overall irradiation programme have established the superiority of the second concept fuel. Comparison of the fractional releases of metallic fission products and particularly the release of iodine underlines the high quality of pyrocarbon coated fuel when dispersed in a silicon carbide matrix.

40. However, so few fission products were released in Charge 13 that further experiments would require much longer times or preferably be done on a much larger scale, for example in an accessible reactor channel, to improve the sensitivity and to establish more accurately the distribution of fission products.

ACKNOWLEDGEMENTS

41. The authors gratefully acknowledge the valuable assistance of the following personnel in designing and evaluating this irradiation programme:

N. Jackson and A. R. Trowell, AERE, Harwell, who were responsible for the operation of the PLUTO loop and the post-irradiation physical examination of the fuel specimens

J. Worth and J. B. Sayers, AERE, Harwell, who were responsible for the ceramographic examination of the PLUTO loop specimens

J. Nairn and D. Livesey, RDL, Windscale, who were responsible for the post-irradiation examination of capsule specimens

C. Lang, RFL, Springfields, and W. Lewis, DMTR, Dounreay, who were responsible for the planning and organisation of DMTR irradiations

Other personnel of the RFL Carbide Dispersed Fuel Development Group.

REFERENCES

1. D'EYE, R. W. M. Dispersed ceramic fuels and the Advanced Gas-cooled Reactor. 1966. UKAEA, TRG Report 1210(S)

2. KENNEDY, P., and SHENNAN, J. The fabrication of UC/SiC dispersed fuels. 1966. UKAEA, TRG Report 1211(S)

TABLE IX

Integrated activities at shutdown and fractional releases - PLUTO 9

(Values given in parentheses correspond with the observed activities less an activity equivalent to the Zr95 found)

Nuclide	Fuel sleeve		Graphite outlet tube		Primary circuit		Complete circuit	
	Integrated activity, μc	Fraction of total activity	Integrated activity, μc	Fraction of total activity	Integrated activity, μc	Fraction of total activity	Integrated activity, μc	Fraction of total activity
Cs134	64	$6{\cdot}75 \times 10^{-4}$	49	$5{\cdot}15 \times 10^{-4}$	220	$2{\cdot}33 \times 10^{-3}$	333	$4{\cdot}4 \times 10^{-3}$
Cs137	919	$1{\cdot}93 \times 10^{-4}$	1,419	$2{\cdot}98 \times 10^{-4}$	5,070	$1{\cdot}40 \times 10^{-3}$	7,408	$2{\cdot}0 \times 10^{-3}$
Sr89	865	$2{\cdot}48 \times 10^{-6}$	-	-	6,760 (6,580)	$1{\cdot}9 \times 10^{-5}$ ($1{\cdot}9 \times 10^{-5}$)	7,625 (7,445)	$2{\cdot}2 \times 10^{-5}$ ($2{\cdot}1 \times 10^{-5}$)
Sr90	12·3	$3{\cdot}5 \times 10^{-6}$	-	-	110 (100)	$3{\cdot}1 \times 10^{-5}$ ($2{\cdot}9 \times 10^{-5}$)	122 (112)	$3{\cdot}5 \times 10^{-5}$ ($3{\cdot}2 \times 10^{-5}$)
Ba140	813 (671)	$1{\cdot}16 \times 10^{-6}$ ($9{\cdot}6 \times 10^{-7}$)	139	$1{\cdot}99 \times 10^{-7}$	6,380 (5,010)	$9{\cdot}6 \times 10^{-6}$ ($7{\cdot}8 \times 10^{-6}$)	7,332 (5,820)	$1{\cdot}1 \times 10^{-5}$ ($8{\cdot}7 \times 10^{-6}$)
Y91	229 (155)	$5{\cdot}82 \times 10^{-7}$ ($3{\cdot}95 \times 10^{-7}$)	175	$4{\cdot}46 \times 10^{-7}$	1,350 (1,270)	$3{\cdot}4 \times 10^{-6}$ ($3{\cdot}2 \times 10^{-6}$)	1,754 (1,600)	$4{\cdot}5 \times 10^{-6}$ ($4{\cdot}1 \times 10^{-6}$)
Ce141	123 (19)	$2{\cdot}2 \times 10^{-7}$ ($3{\cdot}4 \times 10^{-8}$)	3·7	$6{\cdot}66 \times 10^{-7}$	940 (480)	$1{\cdot}7 \times 10^{-6}$ ($8{\cdot}6 \times 10^{-7}$)	1,067 (503)	$1{\cdot}9 \times 10^{-6}$ ($9{\cdot}0 \times 10^{-7}$)
Ce144	11 (0·1)	$8{\cdot}86 \times 10^{-8}$ ($8{\cdot}0 \times 10^{-9}$)	4·1	$3{\cdot}3 \times 10^{-8}$	85 (42)	$6{\cdot}8 \times 10^{-7}$ ($3{\cdot}4 \times 10^{-7}$)	100 (46)	$8{\cdot}0 \times 10^{-7}$ ($3{\cdot}7 \times 10^{-7}$)
Zr95	73·0	$1{\cdot}62 \times 10^{-7}$	16·6	$4{\cdot}2 \times 10^{-8}$	330	$8{\cdot}3 \times 10^{-7}$	420	$1{\cdot}06 \times 10^{-6}$
Te129m	13·0 (6·0)	$4{\cdot}2 \times 10^{-7}$ ($1{\cdot}94 \times 10^{-7}$)	18	$5{\cdot}8 \times 10^{-7}$	300 (290)	$1{\cdot}1 \times 10^{-5}$ ($1{\cdot}0 \times 10^{-5}$)	331 (314)	$1{\cdot}1 \times 10^{-5}$ ($1{\cdot}05 \times 10^{-5}$)
I131	108,900 (106,500)	$3{\cdot}24 \times 10^{-4}$ ($3{\cdot}16 \times 10^{-4}$)	4,825	$1{\cdot}43 \times 10^{-5}$	12,300 (11,900)	$3{\cdot}9 \times 10^{-5}$ ($3{\cdot}6 \times 10^{-5}$)	126,025 (123,225)	$3{\cdot}8 \times 10^{-4}$ ($3{\cdot}7 \times 10^{-4}$)

TABLE X

Activities on fuel sleeve at shutdown - PLUTO 9

(Values given in parentheses correspond with observed activities less an activity equivalent to the Zr95 found)

Nuclide	Activity ($\mu c/cm^2$) for samples						Integrated activity, μc	Fraction of total activity on fuel sleeve
Code	8	10	11	12	13	14		
Description	1 in. stainless-steel section opposite fuel pins:							
	Beginning of fuel sleeve*	13	22	15	8	11		
Area swept by gas, cm^2	0	123	229	441	546	652		
Temp., °C	300	280-420	310-460	380-580	410-630	440-660		
Cs134	<0·001	0·0028	0·011	0·14	0·19	0·23	64·0	$6{\cdot}75 \times 10^{-4}$
	(No significant change on correction for contamination)							
Cs137	0·008	0·062	0·24	2·3	3·1	4·1	919	$1{\cdot}93 \times 10^{-4}$
	(No significant change on correction for contamination)							
Sr89	0·22	-	2·0	-	-	1·1	865	$2{\cdot}48 \times 10^{-6}$
	(No significant change on correction for contamination)							
Sr90	0·0045	-	0·022	-	-	0·020	12·3	$3{\cdot}5 \times 10^{-6}$
	(No significant change on correction for contamination)							
Ba140	0·116	2·07	1·66	1·01	0·512	1·09	813	$1{\cdot}16 \times 10^{-6}$
	(0·086)	(1·72)	(1·43)	(0·93)	(0·487)	(0·62)	(671)	($9{\cdot}6 \times 10^{-7}$)
Y91	0·123	0·604	0·452	0·247	0·164	0·348	229	$5{\cdot}82 \times 10^{-7}$
	(0·105)	(0·399)	(0·315)	(0·198)	(0·149)	(0·075)	(155)	($3{\cdot}95 \times 10^{-7}$)
Ce141	0·041	0·213	0·153	0·105	0·131	0·396	123·2	$2{\cdot}2 \times 10^{-7}$
	(0·018)	(<0·001)	(<0·001)	(0·04)	(0·111)	(0·032)	(18·9)	($3{\cdot}4 \times 10^{-8}$)
Ce144	0·012	0·034	0·028	0·011	0·003	0·006	11·0	$8{\cdot}86 \times 10^{-8}$
	(0·007)	(0)	(0)	(0)	(0)	(0)	(0·1)	($8{\cdot}0 \times 10^{-8}$)
Zr95	0·0193	0·224	0·15	0·0535	0·016	0·30	73·0	$1{\cdot}62 \times 10^{-7}$
Te129m	0·01	0·0113	0·0102	0·0077	0·0272	0·0488	13·0	$4{\cdot}2 \times 10^{-7}$
	(0·0087)	(0)	(0·0001)	(0·0041)	(0·0261)	(0·0285)	(6·0)	($1{\cdot}94 \times 10^{-7}$)
I131	<0·0638	14·7	22·9	166	1,100	66·3	108,900	$3{\cdot}24 \times 10^{-4}$
	(<0·0494)	(13·0)	(21·8)	(166)	(1,100)	(64·0)	(106,500)	($3{\cdot}16 \times 10^{-4}$)

*Activity at this point is taken to be that for the inner end of the pressure vessel shield (P9/8).

TABLE XI

Activities in graphite outlet tube - PLUTO 9

(Values given in parentheses correspond with observed activities less an activity equivalent to the Zr95 found)

Nuclide	Activity ($\mu c/cm^2$) for samples							Integrated activity, μc	Fraction of total activity in graphite outlet tube
Code	15	16	17	18	19	20	1		
Description	½ in. dia. trepanned disc from wall of graphite outlet tube - distance from fuel carrier end:								
	5cm	10cm	15cm	20cm	25cm	30cm	End of outlet tube*		
Area swept by gas, cm^2	740	774	809	843	878	902	953		
Temp. °C	600-700	600-650	~600	~600	~600	~600	600-700		
Cs134	0·22	0·20	0·19	0·19	0·19	0·22	0·25	49	$5{\cdot}15 \times 10^{-4}$
	(No significant change on correction for contamination)								
Cs137	5·0	4·6	5·0	5·3	5·6	6·8	5·0	1419	$2{\cdot}98 \times 10^{-4}$
	(No significant change on correction for contamination)								
Sr89	-	-	-	-	-	-	-	-	-
Sr90	-	-	-	-	-	-	-	-	-
Ba140	0·624	0·499	0·526	0·401	0·485	0·443	0·554	139	$1{\cdot}99 \times 10^{-7}$
	(No significant change on correction for contamination)								
Y91	0·355	0·451	0·577	1·33	0·281	-	0·131	175	$4{\cdot}46 \times 10^{-7}$
	(No significant change on correction for contamination)								
Ce141	2·00	2·74	1·78	1·93	1·33	1·33	0·075	373	$6{\cdot}66 \times 10^{-7}$
	(No significant change on correction for contamination)								
Ce144	<0·007	0·044	0·007	0·015	0·007	<0·007	0·005	4·1	$3{\cdot}3 \times 10^{-8}$
	(No significant change on correction for contamination)								
Zr95	-	-	-	-	-	-	0·015	16·6	$4{\cdot}2 \times 10^{-8}$
Te129m	-	-	-	-	-	-	0·10	18	$5{\cdot}8 \times 10^{-7}$
I131	0·89	11·9	1·05	<0·124	0·298	2·63	0·0147	4825	$1{\cdot}43 \times 10^{-5}$
	(No significant change on correction for contamination)								

*Activity at this point is taken to be that for the Dumbell flag (P9/1).

TABLE XII

Activities in primary circuit at shutdown - PLUTO 9

(Values in parentheses correspond with observed activities less an activity equivalent to the Zr95 found)

Nuclide	Activity ($\mu c/cm^2$) for samples							Integrated activity, μc	Fraction of total activity in primary circuit
Code	1	3	4	5	6	7	8		
Description	Dumbell flag (st. steel)	He outlet mid shield plug (st. steel)	He outlet outside shield plug (st. steel)	He inlet outside shield plug (st. steel)	Inlet flag (st. steel)	Shield mid fuel section (st. steel)	Shield inner end (st. steel)		
Area swept by gas, cm^2	0	750	1,500	14,000	15,500	22,000	28,500		
Temp., °C	600-700	400	300	100	150	250	300		
Cs134	0·25	0·024	0·032	0·00041	0·0023	<0·0018	<0·0010	220	$2·9 \times 10^{-3}$
Cs137	0·50	0·54	0·76	0·014	0·027	<0·0068	0·0080	5,070	$1·40 \times 10^{-3}$
Sr89	0·925	0·50	0·47	0·47	0·28	0·080	0·091	6,760	$1·9 \times 10^{-5}$
Sr90	0·026	0·01	0·0084	0·005	0·0054	0·00086 (0·00042)	0·0018 (0·0016)	110 (100)	$3·1 \times 10^{-5}$ ($2·9 \times 10^{-5}$)
Ba140	0·554	0·291	0·291	0·374	0·208	0·0457	0·161 (0·086)	6,380 (5,010)	$9·6 \times 10^{-6}$ ($7·8 \times 10^{-6}$)
Y91	0·13	0·18	0·17	0·15	0·097 (0 ·090)	0·12 (0·11)	0·12 (0·11)	1,350 (1,270)	$3·4 \times 10^{-6}$) ($3·2 \times 10^{-6}$)
Ce141	0·075 (0·055)	0·049 (0·040)	0·051 (0·045)	0·29	0·026 (0·022)	0·062 (0·011)	0·041 (0·016)	940 (480)	$1·7 \times 10^{-6}$ ($8·6 \times 10^{-7}$)
Ce144	0·0053 (0·001)	0·0049 (0·0036)	0·0032 (0·0023)	0·016	0·0018 (0·001)	<0·006 (0)	0·012 (0·007)	55 (42)	$6·8 \times 10^{-7}$ ($3·4 \times 10^{-7}$)
Zr95	0·0160	0·00535	0·00364	<0·00097	0·0030	0·0377	0·0193	330	$8·0 \times 10^{-7}$
Te129m	0·01	0·0261	0·017	0·00094	<0·00182 (<0·0016)	0·0295 (0·026)	0·010 (0·0087)	300 (290)	$1·1 \times 10^{-5}$ ($1·0 \times 10^{-5}$)
I131	0·0147	0·27	4·4	0·0165	0·0615 (0·0593)	<0·103 (<0·060)	<0·0638 (<0·0494)	12,300 (11,900)	$3·7 \times 10^{-5}$ ($3·6 \times 10^{-5}$)

TABLE XIII

Integrated activities and fractional releases - PLUTO 10

(Values in parentheses correspond with the observed activities less an activity equivalent to the Zr95 found)

Nuclide	Fuel sleeve		Graphite outlet tube		Primary circuit		Complete circuit	
	Integrated activity, μc	Fraction of total activity	Integrated activity, μc	Fraction of total activity	Integrated activity, μc	Fraction of total activity	Integrated activity, μc	Fraction of total activity
Cs134	24·0	$1{\cdot}95 \times 10^{-4}$	19·3	$1{\cdot}57 \times 10^{-4}$	210	$1{\cdot}7 \times 10^{-3}$	253	$2{\cdot}05 \times 10^{-3}$
Cs137	406·6 (401·0)	$1{\cdot}1 \times 10^{-4}$ ($1{\cdot}09 \times 10^{-4}$)	218·7	$5{\cdot}92 \times 10^{-8}$	3,160	$8{\cdot}6 \times 10^{-4}$	3,785 (3,780)	$1{\cdot}02 \times 10^{-3}$ ($1{\cdot}02 \times 10^{-3}$)
Sr89	263·8 (51·0)	$8{\cdot}6 \times 10^{-7}$ ($1{\cdot}66 \times 10^{-7}$)	29·22 (14·44)	$9{\cdot}53 \times 10^{-8}$ ($4{\cdot}71 \times 10^{-8}$)	1,420 (900)	$4{\cdot}6 \times 10^{-6}$ ($2{\cdot}9 \times 10^{-6}$)	1,713 (965)	$5{\cdot}59 \times 10^{-6}$ ($3{\cdot}15 \times 10^{-6}$)
Sr90	7·5 (4·1)	$2{\cdot}12 \times 10^{-6}$ ($1{\cdot}16 \times 10^{-6}$)	1·9 (1·7)	$5{\cdot}38 \times 10^{-7}$ ($4{\cdot}83 \times 10^{-7}$)	120	$3{\cdot}4 \times 10^{-5}$	129 (126)	$3{\cdot}65 \times 10^{-5}$ ($3{\cdot}57 \times 10^{-5}$)
Ba140	359·6 (19·0)	$5{\cdot}98 \times 10^{-7}$ ($3{\cdot}16 \times 10^{-8}$)	25·2 (<1·0)	$4{\cdot}18 \times 10^{-8}$ ($1{\cdot}6 \times 10^{-9}$)	<1,830 (<880)	$3{\cdot}0 \times 10^{-6}$ ($1{\cdot}5 \times 10^{-6}$)	<2,215 (<900)	$3{\cdot}68 \times 10^{-6}$ ($1{\cdot}5 \times 10^{-6}$)
Y91	195·0 (<3·0)	$5{\cdot}58 \times 10^{-7}$ ($8{\cdot}6 \times 10^{-9}$)	-	-	630 (200)	$1{\cdot}8 \times 10^{-6}$ ($6{\cdot}0 \times 10^{-7}$)	825 (203)	$2{\cdot}36 \times 10^{-6}$ ($5{\cdot}8 \times 10^{-7}$)
Ce141	303·3 (<4·9)	($6{\cdot}28 \times 10^{-7}$) ($1{\cdot}0 \times 10^{-8}$)	692·0	$1{\cdot}43 \times 10^{-6}$	350 (0)	$7{\cdot}0 \times 10^{-7}$ (0)	1,345 (706)	$2{\cdot}79 \times 10^{-6}$ ($1{\cdot}46 \times 10^{-6}$)
Ce144	71·45 (0)	$5{\cdot}9 \times 10^{-7}$ (0)	4·0 (<0·04)	$3{\cdot}3 \times 10^{-8}$ ($<3{\cdot}3 \times 10^{-10}$)	150 (16)	$1{\cdot}2 \times 10^{-6}$ ($1{\cdot}3 \times 10^{-7}$)	226 (16)	$1{\cdot}87 \times 10^{-6}$ ($1{\cdot}32 \times 10^{-7}$)
Zr95	248·5	$6{\cdot}99 \times 10^{-7}$	14·9	$4{\cdot}19 \times 10^{-8}$	530	$1{\cdot}5 \times 10^{-6}$	793	$2{\cdot}23 \times 10^{-6}$
Te129m	505·6 (497·0)	$1{\cdot}95 \times 10^{-5}$ ($1{\cdot}92 \times 10^{-5}$)	172·9	$6{\cdot}67 \times 10^{-6}$	2,020 (2,000)	$7{\cdot}8 \times 10^{-5}$ ($7{\cdot}8 \times 10^{-5}$)	2,699 (2,670)	$1{\cdot}04 \times 10^{-4}$ ($1{\cdot}03 \times 10^{-4}$)
I131	112,640	$3{\cdot}64 \times 10^{-4}$	373·6	$1{\cdot}2 \times 10^{-6}$	20,810 (20,240)	$6{\cdot}7 \times 10^{-5}$ ($6{\cdot}5 \times 10^{-5}$)	133,824 (133,254)	$4{\cdot}33 \times 10^{-4}$ ($4{\cdot}31 \times 10^{-4}$)

TABLE XIV

Activities on the fuel carrier sleeve at shutdown - PLUTO 10

(Values in parentheses correspond with the observed activities less an activity equivalent to the Zr95 found)

Nuclide	Activity ($\mu c/cm^2$) for samples							Integrated activity, μc	Fraction of total activity in fuel sleeve
Code	7	8	9	10	11	12	13		
Description	Beginning of fuel sleeve*	1 cm dia. stainless-steel pipe opposite fuel pins: 6	5	11	3	2	1		
Area swept by gas, cm^2	0	58	175	292	409	526	643		
Temp., °C	300	325	350	400	460	520	550		
Cs134	0·0023	<0·0056	0·0065	0·0049	0·049	0·16	0·027	24·0	$1·95 \times 10^{-4}$
	(No significant change on correction for contamination)								
Cs137	0·048	0·019 (0·015)	0·038 (0·038)	0·088 (0·066)	0·70 (0·70)	2·7 (2·7)	0·43 (0·43)	406·6 (401·0)	$1·1 \times 10^{-4}$ $(1·09 \times 10^{-4})$
Sr89	0·016 (0·013)	0·48 (0·11)	0·14 (0·10)	2·1 (0·3)	0·27 (0)	0·16 (0·08)	0·094 (0·01)	263·8 (51·0)	$8·6 \times 10^{-7}$ $(1·66 \times 10^{-7})$
Sr90	0·0014 (0·0014)	0·008 (0·004)	0·008 (0·008)	0·028 (0·007)	0·009 (0·005)	0·009 (0·008)	0·01 0·009	7·5 4·1	$2·12 \times 10^{-6}$ $(1·16 \times 10^{-6})$
Ba140	<0·035 (<0·029)	0·94 (0·21)	0·089 (0·006)	3·70 (0·15)	0·35 (0)	<0·085 (0)	0·073 (0)	359·6 (19·0)	$5·98 \times 10^{-7}$) $(3·16 \times 10^{-8})$
Y91	0·007 (0·003)	0·41 (0)	0·060 (0·012)	2·10 0·04	0·20 (0)	<0·04 (0)	0·023 (0)	195·0 (<3·0)	$5·58 \times 10^{-7}$ $(8·6 \times 10^{-9})$
Ce141	-	0·48 (0)	0·17 0·10	2·6 (0)	0·17 (0)	<0·09 (0)	0·079 (0)	303·3 (<4·9)	$6·28 \times 10^{-7}$ $(1·0 \times 10^{-8})$
Ce144	-	0·12 (0)	0·016 (0)	0·69 (0)	0·063 (0)	0·009 (0)	0·022 (0)	71·45 (0)	$5·9 \times 10^{-7}$ (0)
Zr95	0·0038	0·43	0·049	2·1	0·37	0·099	0·093	248·5	$6·99 \times 10^{-7}$
Te129m	0·0053 (0·0053)	0·030 (0)	0·038 (0·034)	0·12 (0)	2·3 (2·3)	2·3 (2·3)	0·35 (0·35)	505·6 (497·0)	$1·95 \times 10^{-5}$ $(1·92 \times 10^{-5})$
I131	0·075 (0·07)	27·6 (No significant change on correction for contamination)	55·7	588	464	24·1	31·0	112,640	$3·64 \times 10^{-4}$

*Activity at this point is taken to be that for the inner end of the pressure vessel shield (P10/7).

TABLE XV

Activities in the graphite outlet tube - PLUTO 10

(Values given in parentheses correspond with the observed activities less an activity equivalent to the Zr95 found)

Nuclide	Activity ($\mu c/cm^2$) for samples							Integrated activity, μc	Fraction of total activity, graphite outlet tube
Code	14	15	16	17	18	19	1		
Description	½ in. dia. trepanned discs from wall of graphite outlet tube - distance from fuel carrier end: 2 cm	5 cm	10 cm	15 cm	20 cm	20 cm	End of outlet tube*		
Area swept by gas, cm^2	720	744	782	820	860	935	950		
Temp., °C	600-650	600-650	600-650	600-650	600-650	600-650	600-700		
Cs134	0·09	0·041	0·067	0·032	0·035	0·090	0·088	19·3	$1{\cdot}57 \times 10^{-4}$
	(No significant change on correction for contamination)								
Cs137	1·4	0·56	0·98	0·49	0·52	1·4	1·8	218·7	$5{\cdot}92 \times 10^{-5}$
	(No significant change on correction for contamination)								
Sr89	0·066 (0·03)	0·041 (0·01)	0·15 (0·10)	0·12 (0·08)	0·09 (0·03)	0·11 (0·05)	0·28 (0·12)	29·22 (14·44)	$9{\cdot}53 \times 10^{-8}$ ($4{\cdot}71 \times 10^{-8}$)
Sr90	0·007 (0·007)	0·004 (0·004)	0·006 (0·005)	0·005 (0·004)	0·006 (0·005)	0·007 (0·006)	0·012 (0·010)	1·9 (1·7)	$5{\cdot}38 \times 10^{-7}$ ($4{\cdot}83 \times 10^{-7}$)
Ba140	0·098 (0·025)	0·090 (0·029)	0·083 (0)	0·090 (0·005)	0·083 (0)	0·12 (0·01)	0·23 (0)	25·2 (<1·0)	$4{\cdot}18 \times 10^{-8}$) ($1{\cdot}6 \times 10^{-9}$)
Y91	-	-	-	-	-	-	-	-	-
Ce141	3·0	2·9	2·9	2·4	3·1	2·5	0·25	692·0	$1{\cdot}43 \times 10^{-6}$
	(No significant change on correction for contamination)								
Ce144	0·017 (0·002)	0·014 (0·002)	0·014 (0)	0·013 (0)	0·015 (0)	0·017 (0)	0·057 (0)	4·0 (<0·04)	$3{\cdot}3 \times 10^{-8}$ ($<3{\cdot}3 \times 10^{-10}$)
Zr95	0·043	0·036	0·060	0·050	0·068	0·067	0·19	14·9	$4{\cdot}19 \times 10^{-8}$
Te129m	0·61	0·35	0·39	0·41	0·43	0·83	1·8	172·9	$6{\cdot}67 \times 10^{-6}$
	(No significant change on correction for contamination)								
I131	2·83	2·68	0·67	0·82	0·82	3·35	0·219	373·6	$1{\cdot}21 \times 10^{-6}$
	(No significant change on correction for contamination)								

*Activity at this point taken to be that for the Dumbell flag (P10/1).

TABLE XVI

Primary circuit activities at shutdown - PLUTO 10

(Values given in parentheses correspond with the observed activities less an activity equivalent to the Zr95 found)

Nuclide	Activity ($\mu c/cm^2$) for samples							Integrated activity, μc	Fraction of total activity in primary circuit
Code	1	2	3	4	5	6	7		
Description	Dumbell flag (st. steel)	He outlet pipe mid shield plug (st. steel)	He outlet pipe outside shield plug (st. steel)	He inlet pipe outside shield plug (st. steel)	Inlet flag (st. steel)	Shield mid fuel section (st. steel)	Shield inner end (st. steel)		
Area swept by gas, cm^2	0	750	1,500	14,000	15,500	22,000	28,500		
Temp., ^oC	600-700	400	300	100	150	250	300		
Cs134	0·088	0·021	0·033	<0·001	<0·0006	<0·0096	0·0023	210	$1·7 \times 10^{-3}$
	(No significant change on correction for contamination)								
Cs137	1·8	0·43	0·84	0·0069	0·0032	0·048	0·048	3,160	$8·6 \times 10^{-4}$
	(No significant change on correction for contamination)								
Sr89	0·28	0·072	0·066	0·054	0·029	0·055	0·016	1,420	$4·6 \times 10^{-6}$
	(0·12	(0·050)	(0·048)	(0·054)	(0·021)	(0)	(0·013)	(900)	$(2·9 \times 10^{-6})$
Sr90	0·012	0·0029	0·0033	0·0017	0·0016	0·017	0·0014	120	$3·4 \times 10^{-5}$
	(0·010)	(0·0027)	(0·0031)	(0·0017)	(0·0016)	(0·017)	(0·0014)	(120)	$(3·4 \times 10^{-5})$
Ba140	0·23	0·054	0·048	0·025	<0·043	<0·21	<0·035	1,830	$3·0 \times 10^{-6}$
	(0)	(0·012)	(0·012)	(0·025)	(<0·027)	(<0·07)	(<0·029)	(880)	$(1·5 \times 10^{-6})$
Y91	0·21	0·037	0·038	0·019	0·017	0·066	0·007	630	$1·8 \times 10^{-6}$
	(0·02)	(0·012)	(0·017)	(0·019)	(0·008)	(0)	(0·003)	(200)	$(6·0 \times 10^{-7})$
Ce141	0·25	0·025	0·022	0·0047	0·0076	0·027	-	350	$7·0 \times 10^{-7}$
	(0)	(0)	(0)	(0·004)	(0)	(0)		(10)	$(2·0 \times 10^{-7})$
Ce144	0·057	0·009	0·0078	0·0018	0·0035	0·019	-	150	$1·2 \times 10^{-6}$
	(0)	(0)	(0·0007)	(0·0016)	(0·0003)	(0)		(16)	$(1·3 \times 10^{-7})$
Zr95	0·19	0·025	0·021	0·0005	0·0095	0·080	0·0038	530	$1·5 \times 10^{-6}$
Te129m	1·8	0·47	0·30	0·0013	0·002	0·026	0·0053	2,020	$7·8 \times 10^{-5}$
	(1·8)	(0·47)	(0·30)	(0·0013)	(0·0013)	(0·020)	(0·0053)	(2,000)	$(7·8 \times 10^{-5})$
I131	0·219	2·58	5·77	0·061	0·088	<0·24	0·075	20,810	$6·7 \times 10^{-5}$
	(0·054)	(2·58)	(5·77)	(0·061)	(0·08)	(<0·17)	(0·07)	(20,240)	$(6·5 \times 10^{-5})$

TABLE XVII

Integrated activities at shutdown and fractional releases - PLUTO 13

(Values given in parentheses correspond with the observed activities less an activity equivalent to the Zr95 found)

Nuclide	Fuel sleeve		Graphite outlet tube		Primary circuit		Complete circuit	
	Integrated activity, μc	Fraction of total activity	Integrated activity, μc	Fraction of total activity	Integrated activity, μc	Fraction of total activity	Integrated activity, μc	Fraction of total activity
Cs134	$<5{\cdot}4$	$<1{\cdot}1 \times 10^{-4}$	$5{\cdot}5$	$1{\cdot}1 \times 10^{-4}$	$<1{\cdot}4$	$<2{\cdot}7 \times 10^{-5}$	$<12{\cdot}3$	$<2{\cdot}4 \times 10^{-4}$
Cs137	$12{\cdot}4$	$3{\cdot}3 \times 10^{-6}$	$17{\cdot}2$	$4{\cdot}6 \times 10^{-6}$	340	$9{\cdot}0 \times 10^{-5}$	370	$9{\cdot}8 \times 10^{-5}$
Sr89	43 (1)	$1{\cdot}1 \times 10^{-7}$ $(2{\cdot}5 \times 10^{-9})$	$6{\cdot}6$ $(2{\cdot}9)$	$1{\cdot}6 \times 10^{-8}$ $(7{\cdot}1 \times 10^{-9})$	$17{\cdot}5$ $(7{\cdot}5)$	$4{\cdot}3 \times 10^{-8}$ $(1{\cdot}8 \times 10^{-8})$	$67{\cdot}1$ $(11{\cdot}4)$	$1{\cdot}6 \times 10^{-7}$ $(2{\cdot}8 \times 10^{-8})$
Sr90	$1{\cdot}5$ $(0{\cdot}7)$	$4{\cdot}2 \times 10^{-7}$ (2×10^{-7})	$1{\cdot}7$	$4{\cdot}7 \times 10^{-7}$	$3{\cdot}1$	$8{\cdot}6 \times 10^{-7}$	$6{\cdot}3$ $(5{\cdot}5)$	$1{\cdot}7 \times 10^{-6}$ $(1{\cdot}5 \times 10^{-6})$
Ba140	$\ll 273$ $(\ll 96{\cdot}4)$	$\ll 3{\cdot}0 \times 10^{-7}$ $(\ll 1{\cdot}1 \times 10^{-7})$	$\ll 113$ $(\ll 107)$	$\ll 1{\cdot}2 \times 10^{-7}$ $(\ll 1{\cdot}2 \times 10^{-7})$	$\ll 1157$ $(\ll 763)$	$\ll 1{\cdot}3 \times 10^{-6}$ $(\ll 8{\cdot}4 \times 10^{-7})$	$\ll 1,543$ $(\ll 966)$	$\ll 1{\cdot}7 \times 10^{-6}$ $(\ll 1{\cdot}1 \times 10^{-6})$
Y91	70 (<3)	$1{\cdot}54 \times 10^{-7}$ $(<6{\cdot}6 \times 10^{-9})$	- -	- -	28 (0)	$(6{\cdot}2 \times 10^{-8})$ (0)	98 (0)	$2{\cdot}2 \times 10^{-7}$ (0)
Ce141	175 (85)	$2{\cdot}5 \times 10^{-7}$ $(1{\cdot}2 \times 10^{-7})$	$\ll 31$ $(\ll 23)$	$\ll 4{\cdot}5 \times 10^{-8}$ $(\ll 3{\cdot}3 \times 10^{-8})$	$4{\cdot}7$ (0)	$6{\cdot}8 \times 10^{-9}$ (0)	211 (108)	$3{\cdot}1 \times 10^{-7}$ $(1{\cdot}6 \times 10^{-7})$
Ce144	$10{\cdot}5$ (0)	$8{\cdot}0 \times 10^{-8}$ (0)	$2{\cdot}2$ $(0{\cdot}8)$	$1{\cdot}7 \times 10^{-8}$ $(6{\cdot}0 \times 10^{-9})$	$3{\cdot}4$ $(0{\cdot}3)$	$2{\cdot}6 \times 10^{-8}$ $(2{\cdot}5 \times 10^{-9})$	$16{\cdot}1$ $(1{\cdot}1)$	$1{\cdot}2 \times 10^{-7}$ $(8{\cdot}4 \times 10^{-9})$
Zr95	126	$2{\cdot}8 \times 10^{-7}$	$3{\cdot}9$	$8{\cdot}6 \times 10^{-9}$	976	$2{\cdot}2 \times 10^{-6}$	$1,106$	$2{\cdot}4 \times 10^{-6}$
Te129m	60 $(57{\cdot}5)$	$1{\cdot}6 \times 10^{-6}$ $(1{\cdot}6 \times 10^{-6})$	$4{\cdot}5$ $(3{\cdot}9)$	$1{\cdot}2 \times 10^{-7}$ $(1{\cdot}1 \times 10^{-7})$	106 (35)	$2{\cdot}9 \times 10^{-6}$ $(9{\cdot}5 \times 10^{-7})$	171 (97)	$4{\cdot}6 \times 10^{-6}$ $(2{\cdot}6 \times 10^{-6})$
I131	$\ll 174$ $(\ll 102)$	$\ll 3{\cdot}7 \times 10^{-7}$ $(\ll 2{\cdot}2 \times 10^{-7})$	$\ll 95{\cdot}4$	$\ll 2{\cdot}0 \times 10^{-7}$	$<1,104$ (<240)	$< 2{\cdot}4 \times 10^{-6}$ $(< 5{\cdot}2 \times 10^{-7})$	$<1,373$ (<437)	$< 2{\cdot}9 \times 10^{-6}$ $(< 9{\cdot}4 \times 10^{-7})$

TABLE XVIII

Activities on fuel sleeve at shutdown - PLUTO 13

(Values given in parentheses correspond with the observed activities less an activity equivalent to the Zr95 found)

Nuclide	Activity ($\mu c/cm^2$) for samples							Integrated activity, μc	Fraction of total activity on fuel sleeve
Code	7	8	9	10	11	12	13		
Description	1 cm. dia. disc from steel fuel sleeve opposite compacts: Beginning of fuel sleeve*	8	7	6	4	3	2		
Area swept by gas, cm^2	0	58	175	292	409	526	643		
Temp., ^oC	~300	260	300	340	380	440	580		
Cs134	<0·0013	<0·012	0·0079	0·0068	<0·010	<0·0089	<0·0044	5·4	$1·1 \times 10^{-4}$
	(No significant change on correction for contamination)								
Cs137	<0·0017	0·030	0·016	0·014	0·017	0·014	0·017	12·4	$3·3 \times 10^{-6}$
	(No significant change on correction for contamination)								
Sr89	0·0025 (0)	0·023 (0)	0·062 (0)	0·051 (0)	0·095 (0·005)	0·068 (0)	0·083 (0)	42 (1)	$1·06 \times 10^{-7}$ ($2·5 \times 10^{-9}$)
Sr90	0·00056 (0·00008)	0·0051 (0·0046)	0·0015 (0·0008)	0·0012 (0·0004)	0·0020 (0·0012)	0·0012 (0)	0·0043 (0·0032)	1·5 (0·7)	$4·2 \times 10^{-7}$ (2×10^{-7})
Ba140	<0·046 (0)	<0·28 (<0·16)	0·20 (0·03)	<0·37 (<0·17)	<0·28 (<0·08)	<0·41 (<0·07)	<0·69 (<0·45)	273 (96·4)	$3·0 \times 10^{-7}$ ($1·06 \times 10^{-7}$)
Y91	0·049 (0)	0·049 (0)	0·12 (0·03)	0·096 (0)	0·12 (0·02)	0·11 (0)	0·093 (0)	70 (<3)	$1·54 \times 10^{-7}$ ($<<0·6 \times 10^{-9}$)
Ce141	<0·033 (0)	<0·23 (<0·142)	<0·30 (<0·17)	<0·31 (<0·16)	<0·21 (<0·06)	<0·36 (<0·09)	<0·19 (<0·01)	175 (85)	$2·5 \times 10^{-7}$ ($1·2 \times 10^{-7}$)
Ce144	0·00061 (0)	0·0090 (0)	0·019 (0)	0·014 (0)	0·019 (0)	0·017 (0)	0·016 (0)	10·5 (0)	$8·0 \times 10^{-6}$ (0)
Zr95	0·061	0·058	0·086	0·098	0·10	0·17	0·12	126	$2·8 \times 10^{-7}$
Te129m	<0·0091 (<0·0043)	<0·051 (<0·051)	<0·080 (<0·080)	<0·044 (<0·036)	<0·15 (<0·15)	<0·12 (<0·11)	0·10 (0·10)	60 (57·5)	$1·6 \times 10^{-6}$ ($1·55 \times 10^{-6}$)
I131	<0·10 (<0·04)	<0·25 (<0·19)	<0·25 (0·16)	<0·25 (<0·15)	<0·25 (<0·15)	<0·25 (<0·08)	<0·25 (<0·13)	174 (102)	$3·7 \times 10^{-7}$ ($2·2 \times 10^{-7}$)

*Activity at this point is taken to be that for the inner end of the pressure vessel shield (P13/7).

TABLE XIX

Activities in graphite outlet tube at shutdown - PLUTO 13

(Values given in parentheses correspond with the observed activities less an activity equivalent to the Zr95 found)

Nuclide	Activity ($\mu c/cm^2$) for samples							Integrated activity, μc	Fraction of total activity in graphite outlet tube
Code	14	15	16	17	18	19	1		
Description	½ in. dia. disc trepanned from graphite outlet tube - distance from fuel carrier end:								
	2cm	5cm	10cm	15cm	20cm	30cm	End of outlet tube*		
Area swept by gas, cm^2	720	744	782	820	860	935	950		
Cs134	0·032	0·029	0·024	0·022	0·019	0·011	0·00072	5·5	$1·1 \times 10^{-4}$
	(No significant change on correction for contamination)								
Cs137	0·090	0·066	0·064	0·075	0·083	0·064	0·055	17·2	$4·6 \times 10^{-6}$
	(No significant change on correction for contamination)								
Sr89	0·026	0·017	0·018	0·028	0·034	0·026	0·04	6·6	$1·6 \times 10^{-6}$
	(0·012)	(0·004)	(0·001)	(0·012)	(0·021)	(0·014)	(0·014)	(2·9)	$(7·1 \times 10^{-9})$
Sr90	0·0055	0·0026	0·0046	0·0083	0·012	0·0059	0·016	1·7	$4·7 \times 10^{-7}$
	(No significant change on correction for contamination)								
Ba140	<0·21	<0·26	<0·17	<0·24	<0·29	<0·36	<0·12	113	$1·24 \times 10^{-7}$
	(<0·18)	(<0·23)	(<0·13)	(<0·21)	(<0·26)	(<0·33)	(<0·062)	(107)	$(1·2 \times 10^{-7})$
Y91	-	-	-	-	-	-	-	-	-
Ce141	<0·075	<0·053	<0·090	0·15	<0·16	<0·11	<0·022	31	$4·5 \times 10^{-6}$
	(<0·05)	(0·032)	(<0·060)	(<0·12)	(<0·13)	(<0·09)	(0)	(23)	$(3·3 \times 10^{-6})$
Ce144	0·0057	0·0055	0·0050	0·013	0·0090	0·0090	0·0023	2·2	$1·7 \times 10^{-6}$
	(0·0011)	(0·0014)	(0)	(0·008)	(0·0046)	(0·0046)	(0)	(0·8)	$(6·0 \times 10^{-9})$
Zr95	0·016	0·014	0·019	0·018	0·015	0·015	0·029	3·9	$8·6 \times 10^{-9}$
Te129m	<0·021	<0·017	<0·025	<0·017	<0·018	<0·016	0·0072	4·5	$1·2 \times 10^{-7}$
	(<0·021)	(<0·017)	(<0·023)	(<0·015)	(<0·017)	(<0·015)	(0·0048)	(3·9)	$(1·1 \times 10^{-7})$
I131	<0·37	<0·45	<0·45	<0·37	<0·37	<0·37	<0·018	95·4	$2·0 \times 10^{-7}$
	(No significant change on correction for contamination)						(0)		

*Activity at this point taken to be that for the Dumbell flag (P13/1).

TABLE XX

Activities in primary circuit at shutdown - PLUTO 13

(Values given in parentheses correspond with the observed activities less an activity equivalent to the Zr95 found).

Nuclide	Activity ($\mu c/cm^2$) for samples							Integrated activity, μc	Fraction of total activity in primary circuit
Code	1	2	3	4	5	6	7		
Description	Dumbell flag	He outlet mid shield plug	He outlet outside shield plug	He inlet outside shield plug	Inlet flag	Shield mid fuel position	Shield inner position		
Area swept by gas, cm^2	0	750	1,500	14,000	15,500	22,000	28,500		
Temp., ^oC							200		
Cs134	0·00072	0·00028	0·00045	<0·00033	<0·00072	<0·0034	<0·0013	1·4	$2·7 \times 10^{-5}$
Cs137	0·055	0·037	0·041	0·0033	0·021	<0·0041	<0·0017	370	$9·0 \times 10^{-5}$
Sr89	0·04 (0·014)	0·008 (0·005)	0·013 (0·010)	0·012 (0·011)	0·028 (0·012)	0·013 (0)	0·0025 (0)	17·5 (7·5)	$4·3 \times 10^{-6}$ $(1·8 \times 10^{-6})$
Sr90	0·016	0·0028	0·0045	0·0013	0·0052	0·0017	0·00056	3·1	$8·6 \times 10^{-7}$
Ba140	<0·12 (<0·06)	<0·029 (<0·022)	<0·045 (<0·038)	<0·047 (<0·044)	<0·068 (<0·032)	<0·23 (0)	<0·046 (0)	1,157 (763)	$1·3 \times 10^{-5}$ $8·4 \times 10^{-7}$
Y91	<0·0087 (0)	<0·0004 (0)	<0·00053 (0)	<0·00056 (0)	<0·0014 (0)	<0·0020 (0)	<0·0917 (0)	28 (0)	$6·2 \times 10^{-6}$ (0)
Ce141	<0·022 (0)	0·0024 (0)	0·00049 (0)	0·0027 (0·0007)	0·011 (0)	<0·032 (0)	<0·033 (0)	4·7 (0)	$6·8 \times 10^{-9}$
Ce144	0·0023 (0)	0·0020 (0·001)	0·0011 (0)	0·0015 (0·0011)	0·011 (0·006)	0·00081 (0)	0·00061 (0)	3·4 (0·3)	$2·6 \times 10^{-6}$ $(2·5 \times 10^{-9})$
Zr95	0·029	0·0033	0·0037	0·0013	0·018	0·12	0·061	976	$2·2 \times 10^{-5}$
Te129m	0·0072 (0·0048)	<0·0011 (<0·0008)	0·0014 (0·0011)	0·0010 (0·0010)	0·0034 (0·0019)	0·0056 (0)	<0·0091 (<0·004)	106 (35)	$2·9 \times 10^{-6}$ $(9·5 \times 10^{-7})$
I131	<0·018 (0)	0·017 (0·014)	0·023 (0·019)	<0·01 (<0·01)	<0·035 (<0·016)	0·11 (0)	<0·10 (0·04)	1,104 (240)	$2·4 \times 10^{-6}$ $(5·2 \times 10^{-7})$

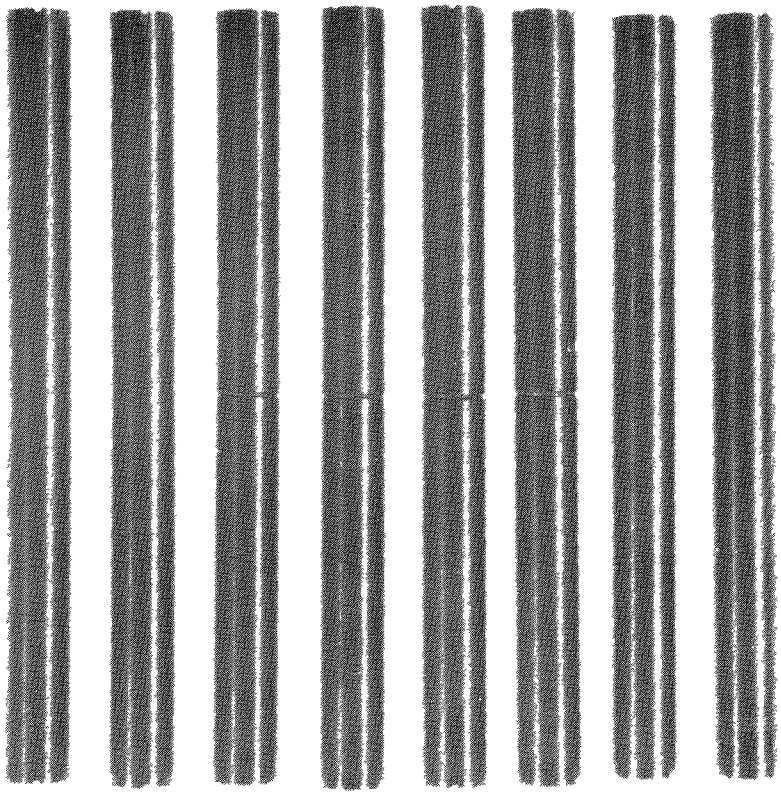

Fig. 1. Rods for PLUTO charge ($x\frac{2}{3}$)

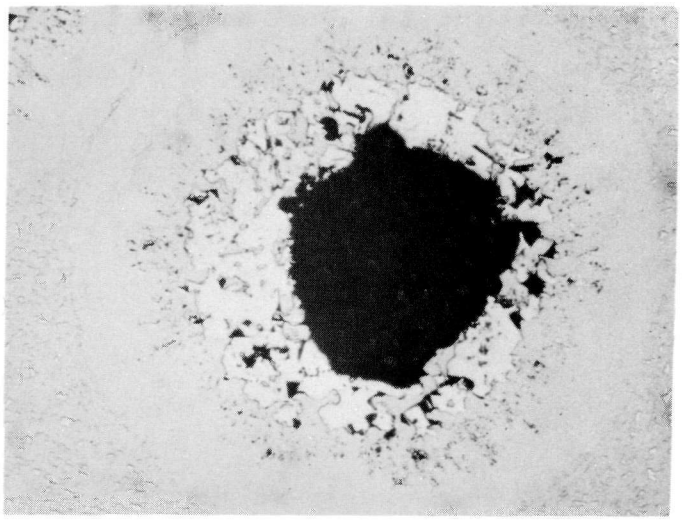

Fig. 2. SiC coated particle in SiC matrix, from PLUTO Charge 9, showing UC/SiC interaction (x100, reduced x $\frac{9}{10}$ in printing)

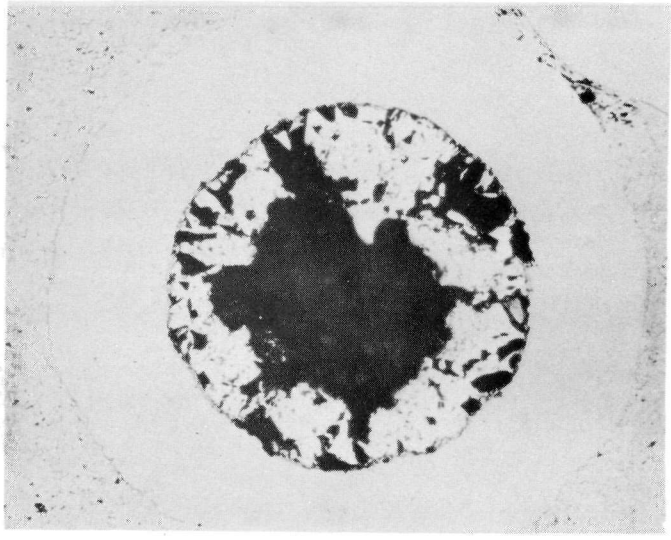

Fig. 3. SiC coated particle in SiC matrix, from PLUTO Charge 10 (x100, reduced x$\frac{9}{10}$ in printing)

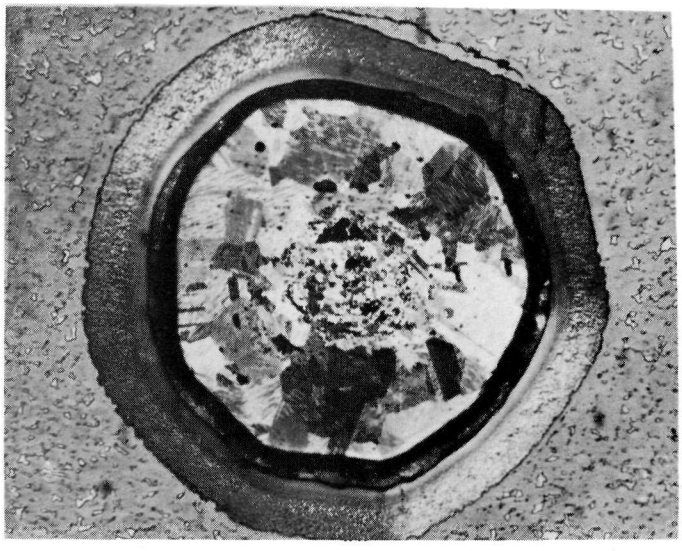

Fig. 4. PyC coated particle in SiC matrix, from PLUTO Charge 13 (x140, reduced x$\frac{9}{10}$ in printing)

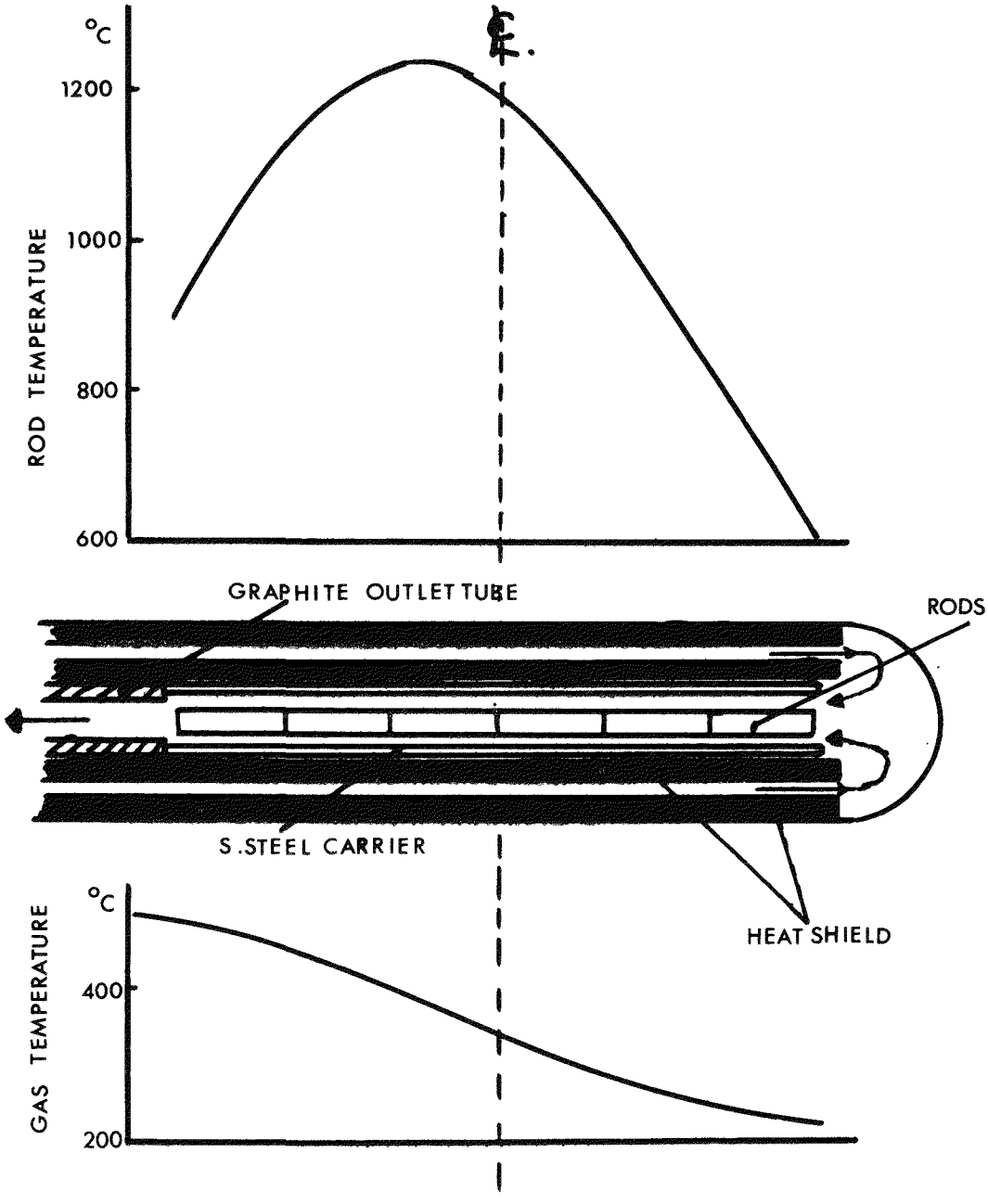

Fig 5 TYPICAL TEMPERATURE DISTRIBUTION IN PLUTO LOOP

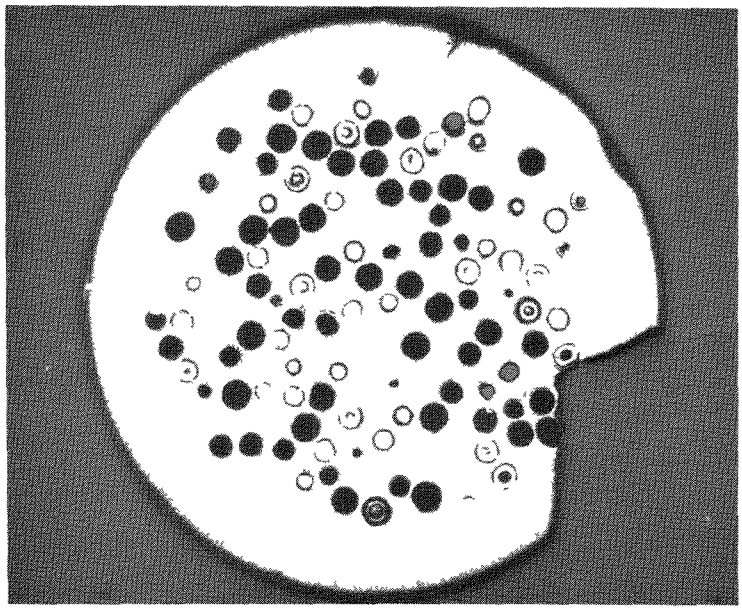

Fig. 6. Cross-section of rod, showing damage caused by silicon melting (x11)

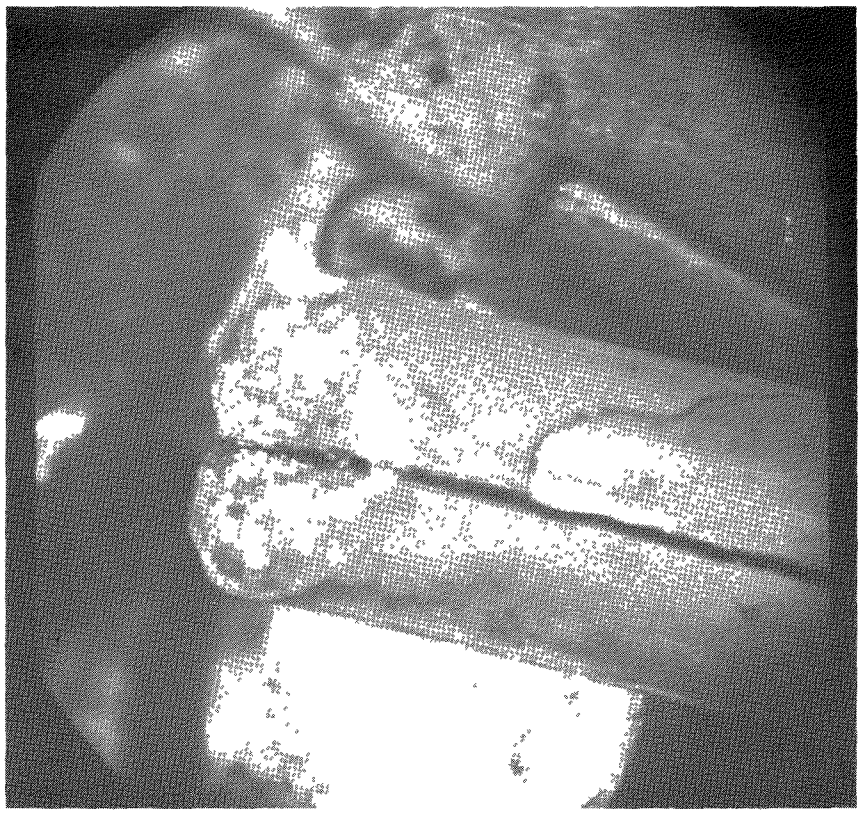

Fig. 7. Damage caused by silicon melting in IE 309/4

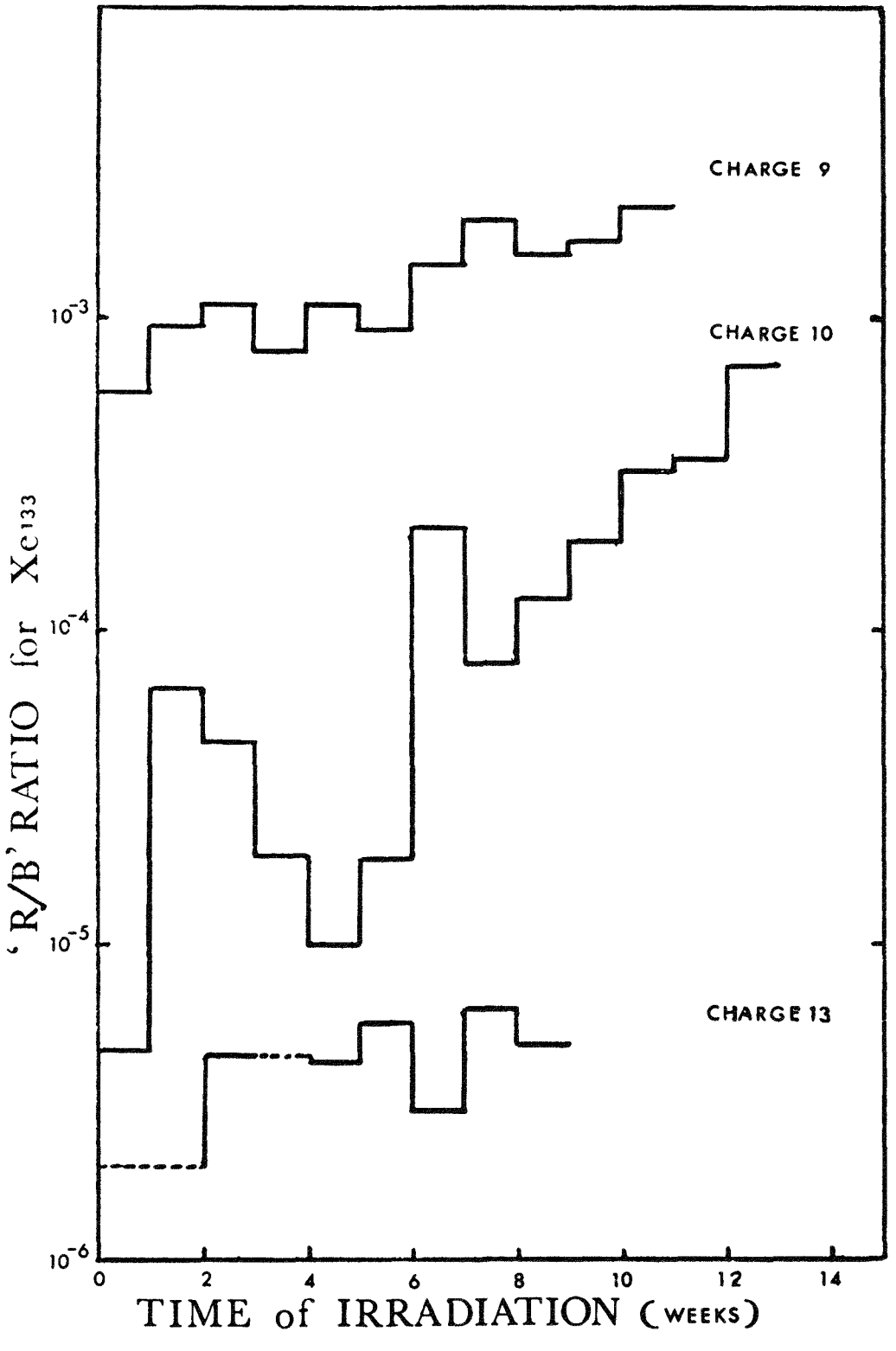

Fig 8 THE VARIATION OF Xe_{133} RELEASE WITH TIME

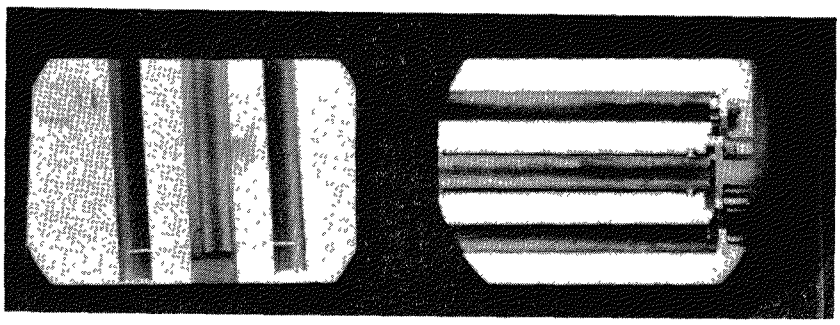

Fig. 9. Surface appearance of rod 11, at helium outlet end in Charge 9 (left, pre-irradiation; right post-irradiation)

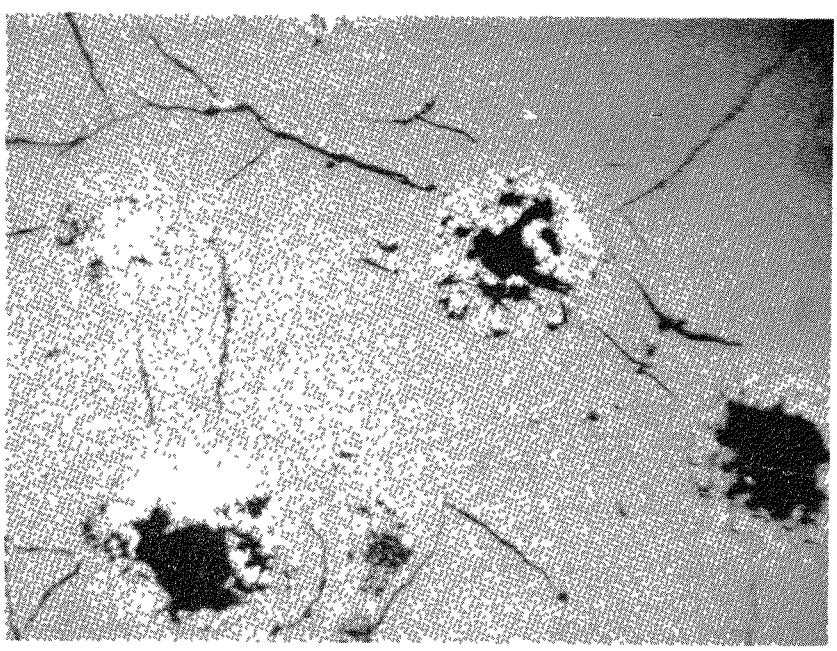

Fig. 10. Cracking caused by irradiation in rod 13, PLUTO Charge 9 (x55)

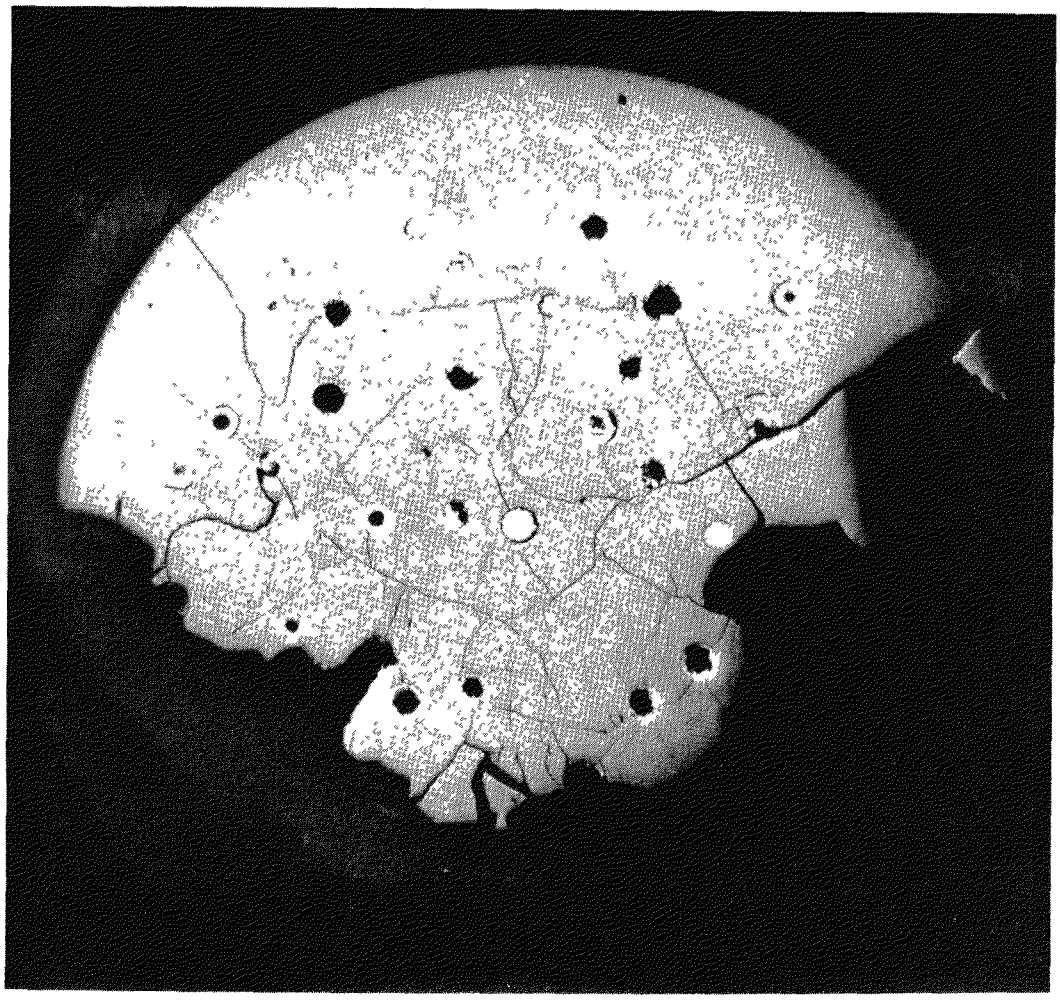

Fig. 11. Effect of irradiation damage in IE 269/6

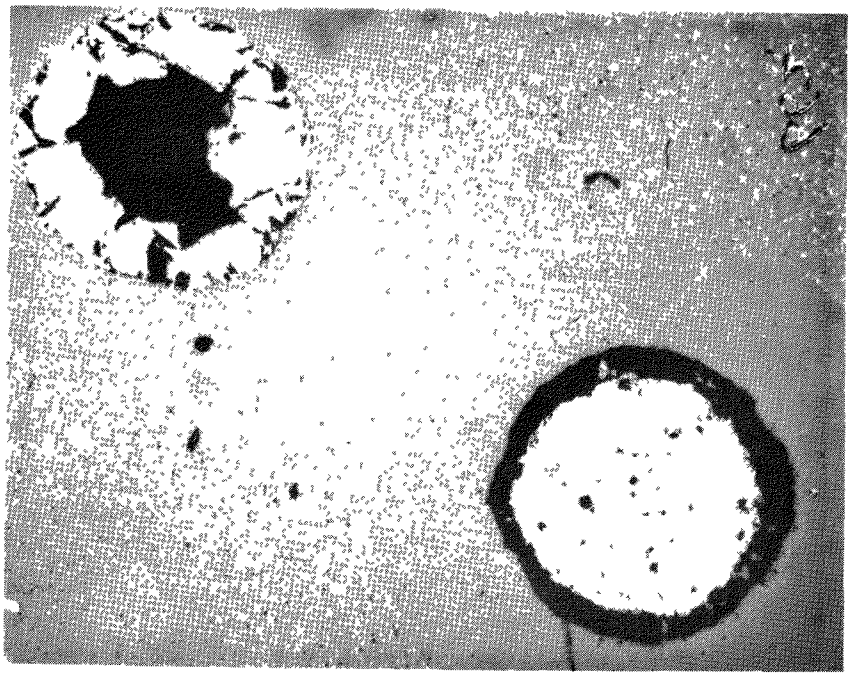

Fig. 12. Section of rod 4, PLUTO Charge 10, after irradiation (x75)

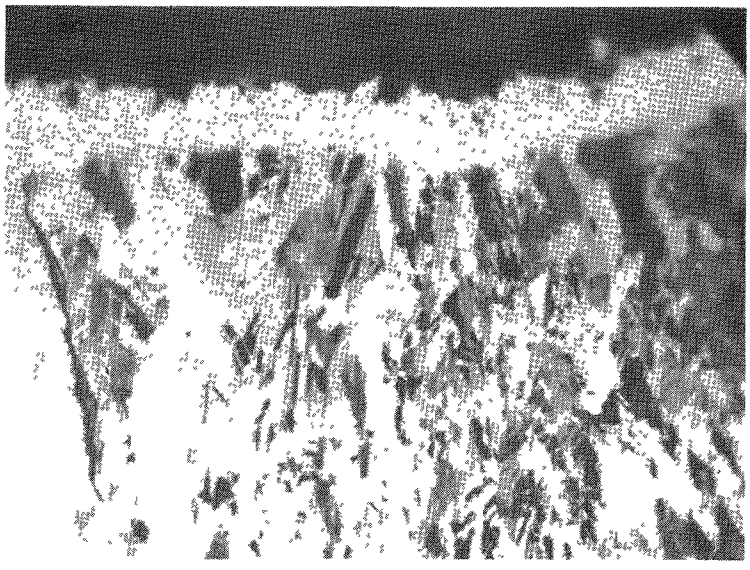

Fig. 13. Fission fragment damaged zone in SiC coating (x1000)

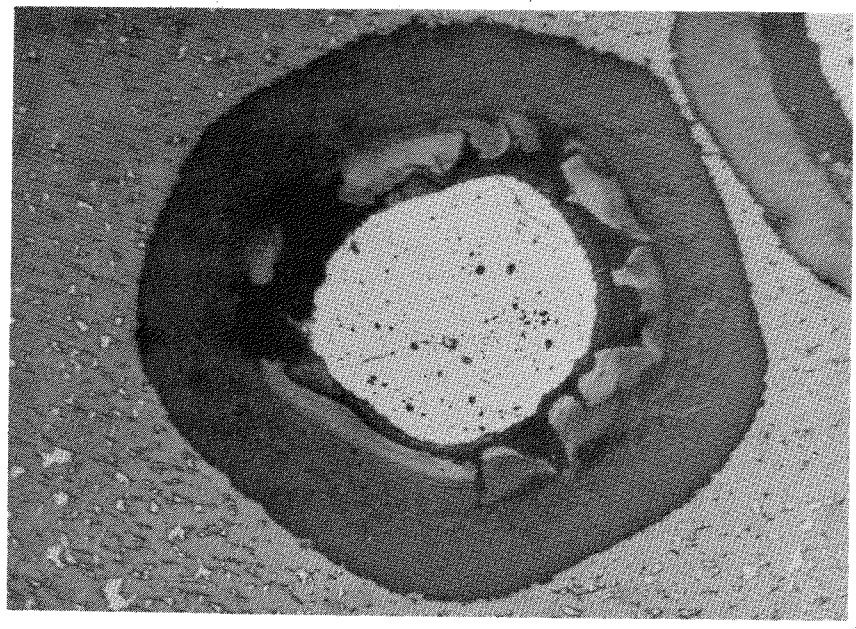

Fig. 14. Irradiation damage to inner pyrocarbon coat (x1000)

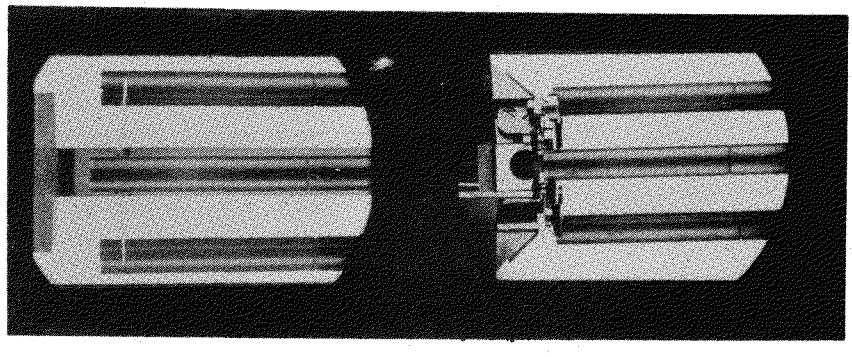

Fig. 15. Surface appearance of rod 8, at helium outlet end in Charge 13 (left, pre-irradiation; right, post-irradiation)

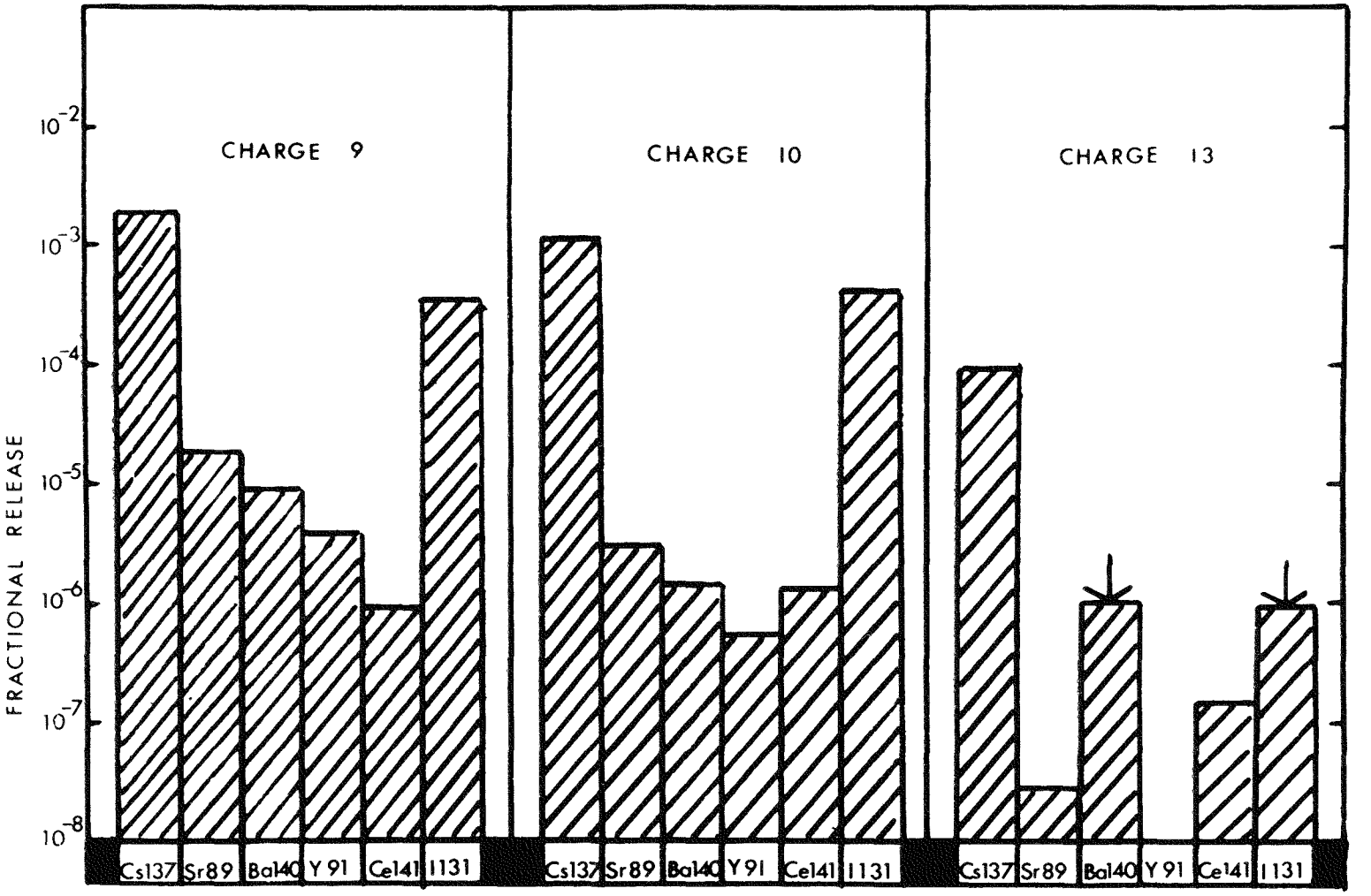

FIG.16. RELEASE OF METAL FISSION PRODUCTS IN PLUTO LOOP

Available from

HER MAJESTY'S STATIONERY OFFICE

49 High Holborn, London W.C.1
423 Oxford Street, London W.1
13a Castle Street, Edinburgh 2
109 St. Mary Street, Cardiff
Brazennose Street, Manchester 2
50 Fairfax Street, Bristol 1
35 Smallbrook, Ringway, Birmingham 5
80 Chichester Street, Belfast

or through any bookseller

Printed in England

S.O. Code No. 91-10